# Synaptotagmin isoforms confer distinct activation kinetics and dynamics to chromaffin cell granules

Tejeshwar C. Rao,[1] Zuleirys Santana Rodriguez,[1] Mazdak M. Bradberry,[2] Alexandra H. Ranski,[1] Peter J. Dahl,[1] Michael W. Schmidtke,[1] Paul M. Jenkins,[1] Daniel Axelrod,[1] Edwin R. Chapman,[2] David R. Giovannucci,[3] and Arun Anantharam[1]

[1]Department of Pharmacology, University of Michigan, Ann Arbor, MI
[2]Howard Hughes Medical Institute, Department of Neuroscience, University of Wisconsin, Madison, WI
[3]Department of Neurosciences, University of Toledo Medical School, Toledo, OH

Adrenomedullary chromaffin cells respond to sympathetic nervous system activation by secreting a cocktail of potent neuropeptides and hormones into the circulation. The distinct phases of the chromaffin cell secretory response have been attributed to the progressive fusion of distinct populations of dense core granules with different activation kinetics. However, it has been difficult to define what distinguishes these populations at the molecular level. Functional segregation of granule pools may depend on selective sorting of synaptotagmin-1 (Syt-1) and synaptotagmin-7 (Syt-7), which our previous work showed are rarely cosorted to the same granule. Here we assess the consequences of selective sorting of Syt isoforms in chromaffin cells, particularly with respect to granule dynamics and activation kinetics. Upon depolarization of cells expressing fluorescent Syt isoforms using elevated $K^+$, we find that Syt-7 granules fuse with faster kinetics than Syt-1 granules, irrespective of stimulation strength. Pharmacological blockade of $Ca^{2+}$ channels reveals differential dependence of Syt-1 versus Syt-7 granule exocytosis on $Ca^{2+}$ channel subtypes. Syt-7 granules also show a greater tendency to fuse in clusters than Syt-1 granules, and granules harboring Syt-1 travel a greater distance before fusion than those with Syt-7, suggesting that there is spatial and fusion-site heterogeneity among the two granule populations. However, the greatest functional difference between granule populations is their responsiveness to $Ca^{2+}$. Upon introduction of $Ca^{2+}$ into permeabilized cells, Syt-7 granules fuse with fast kinetics and high efficacy, even at low $Ca^{2+}$ levels (e.g., when cells are weakly stimulated). Conversely, Syt-1 granules require a comparatively larger increase in intracellular $Ca^{2+}$ for activation. At $Ca^{2+}$ concentrations above 30 µM, activation kinetics are faster for Syt-1 granules than for Syt-7 granules. Our study provides evidence for functional specialization of chromaffin cell granules via selective expression of Syt isoforms with different $Ca^{2+}$ sensitivities.

## INTRODUCTION

Regulated exocytosis in chromaffin cells is triggered by membrane depolarization and subsequent $Ca^{2+}$ influx through voltage-gated channels. The level of $Ca^{2+}$ accumulation is commensurate with the strength of stimulation (Douglas and Rubin, 1961; Neher and Augustine, 1992; Fulop and Smith, 2007; de Diego et al., 2008). $Ca^{2+}$ drives exocytosis through the $Ca^{2+}$-binding synaptotagmin (Syt) protein family (Brose et al., 1992; Voets et al., 2001a; Schonn et al., 2008). The Syt protein family includes 17 isoforms, but only two of these isoforms (Syt-1 and Syt-7) are known to be expressed on chromaffin cell dense core granules (Schonn et al., 2008). Both Syt isoforms harbor an N-terminal transmembrane domain that extends into the lumen of the chromaffin granule, followed by two cytosolic C2 domains (C2A and C2B) connected by a short linker region (Perin et al., 1990, 1991; Chapman, 2002). The $Ca^{2+}$- and membrane-binding properties of these isoforms are determined primarily by the amino acid sequence within the tandem C2 domains (Sutton et al., 1995; Ubach et al., 1998; Fernandez et al., 2001). Biochemical studies have established several differences in how these isoforms respond to $Ca^{2+}$. For example, Syt-7 is capable of binding a total of six $Ca^{2+}$ ions, while Syt-1 can bind to only five (Südhof and Rizo, 1996; Ubach et al., 1998). Although both proteins bind membranes in a $Ca^{2+}$-dependent manner, Syt-7 does so with a 10-fold higher sensitivity for $Ca^{2+}$ ions compared with Syt-1 (Sugita et al., 2002; Bhalla et al., 2005).

The notion that granule or vesicle proteins may confer spatiotemporal heterogeneity to fusion events has recently become more widely appreciated. At synapses, there is evidence that vesicle-associated membrane protein/synaptobrevin isoforms may act to sort vesicles into synchronous, asynchronous, and spontaneously fusing populations (Raingo et al., 2012; Bal et al., 2013; Crawford and Kavalali, 2015). Syt isoforms may serve similar

Correspondence to Arun Anantharam: arunanan@umich.edu
Abbreviations used: NPY, neuropeptide Y; PSS, physiological salt solution; Syt, synaptotagmin; TIRF, total internal reflection fluorescence.



The Rockefeller University Press
J. Gen. Physiol. 2017
https://doi.org/10.1085/jgp.201711757

Supplemental material can be found at:
http://doi.org/10.1085/jgp.201711757

functions in neurons and neuroendocrine cells (Walter et al., 2011; Raingo et al., 2012; Bacaj et al., 2013; Bal et al., 2013; Weber et al., 2014; Crawford and Kavalali, 2015; Lee and Littleton, 2015; Luo et al., 2015). In chromaffin cells, Syt-1 and Syt-7 are thought to drive the bulk of $Ca^{2+}$-triggered exocytosis. When both isoforms are eliminated, the overall secretory capacity of the cell is reduced by greater than 70% (Schonn et al., 2008). Elimination of one isoform at a time revealed that Syt-7 likely accounts for the slow phase of exocytotic release (as revealed by membrane capacitance measurements), while Syt-1 likely accounts for the fast phase (Schonn et al., 2008).

The biochemical differences between Syt-1 and Syt-7 may endow granules with different functional properties during exocytosis. Previous work from our group demonstrated that Syt-1 and Syt-7 are sorted to different populations of chromaffin granules (Rao et al., 2014). Syt-7 granule fusion is triggered by milder membrane depolarization than Syt-1 granule fusion, and fusion pores of granules harboring Syt-1 expand more rapidly than pores of granules expressing Syt-7. Although the underlying mechanisms of these phenomena are unclear, they may result from differential affinities of Syt isoforms for $Ca^{2+}$, phospholipids, and/or effector proteins. The striking differences observed between Syt-1 and Syt-7 granules motivated the work described here, which further clarifies the nature of Syt-mediated differences in granule properties.

In this study, we assessed whether the distinct dynamics and activation kinetics of chromaffin granules could be attributed to the selective sorting of Syt isoforms. Our data reveal that although the cytosolic distribution of granules bearing Syt-1 or Syt-7 is largely overlapping, their mean distances from the membrane were not identical. Although "newcomer" (i.e., vesicles not evident in the evanescent field at the start of stimulation) fusion events accounted for a relatively small percentage of total fusion events, their number was greater for granules with Syt-1 than Syt-7. Syt-1 granules also exhibited a greater tendency to fuse when chromaffin cells were repeatedly challenged with a strongly depolarizing stimulus, suggesting differences in their fusion "readiness" or, potentially, differences in their distribution with respect to sites of exocytosis on the membrane. Indeed, image analysis reveals that Syt-7 granules tend to fuse in clusters, whereas fusion locations of Syt-1 granules are more dispersed. The two populations of granules were also differentially dependent on $Ca^{2+}$ channel subtypes for fusion, consistent with the theme of exocytotic site heterogeneity. Strikingly, the two granule populations responded differentially to increases in cytoplasmic $Ca^{2+}$. Direct cytosolic introduction of $Ca^{2+}$ at defined concentrations demonstrated that the Syt-7 granule population is likely to drive the bulk of exocytosis when cells are weakly stimulated. Syt-1 granules required a comparatively much larger increase in intracellular $Ca^{2+}$ for fusion. At the highest concentrations of $Ca^{2+}$ tested, comparable to a strongly depolarizing electrophysiological stimulus, Syt-1 granules fused with faster kinetics than Syt-7 granules. Overall, these findings demonstrate that chromaffin granules are not homogeneous but are composed of at least two populations with distinct functional properties specified by different Syt isoforms and their responses to $Ca^{2+}$.

## MATERIALS AND METHODS

### Chromaffin cell preparation and transfection

The chromaffin cells used for these experiments were isolated from the adrenal medullae of adult cows (*Bos taurus*) obtained from JBS Packing Company. Transient transfections were performed as described earlier (Wick et al., 1993). In brief, cells were plated on 35-mm glass-bottom tissue culture dishes (refractive index 1.51; World Precision Instruments) precoated with poly-D-lysine and bovine collagen. Cells were transiently transfected by electroporation using the Neon transfection system (Invitrogen). After standardization of the electroporation protocol, the chromaffin cells were transfected with the desired plasmid(s) with a single pulse of 1,100 mV for a period of 40 ms. The media on the cells were changed after overnight incubation, and all the experiments were performed 48 h after transfection to ensure expression of the fusion protein. All procedures were performed after approval was obtained from the Institutional Animal Care and Use Committee.

All fluorescent proteins fused to Syt were located upstream of the N-terminal lumenal domain. For cargo proteins (e.g., neuropeptide Y [NPY]), the fluorescent protein followed the C-terminal region. The parent NPY plasmid was a gift of Wolfhard Almers (Vollum Institute, Portland, OR). All Syt constructs used were made in pCI vectors with coding sequences from *Rattus norvegicus*. The linker sequence between the upstream fluorescent protein tag for both Syts is 5′-GAATTCTAG ACAGGCGGAAGCGGAGGCTCCGGCGGGAGCGGC GGA-3′. A bovine preprolactin signal sequence is located further upstream of the pHluorin/GFP/pHuji tag. The pHluorin and pHuji tags can be removed from the plasmid by cutting with upstream (Acc65I, KpnI, or MluI) and downstream (XbaI) enzymes. The GFP used here is the "enhanced" GFP variant.

### Immunocytochemistry

Immunofluorescence microscopy was performed to detect the distribution of Syt isoforms within chromaffin cells. Cells were first fixed with 4% PFA in PBS for 30 min at 37°C. The cells were quickly rinsed after the incubation and quenched in a solution of 50 mM $NH_4Cl$ in PBS for 30 min at 37°C. After washing off the quenching solution, the cells were permeabilized using acetone

solution for 7 min. After the incubation, the cells were washed with TBS twice and blocked with 1% gelatin in TBS for 20 min, followed by 4% donkey serum for 30 min, both at 37°C. A solution of 2–4 mg/ml BSA made in TBS was used to dilute the primary and secondary antibodies. Cells were incubated for 2 h at 37°C with a combination of the following primary antibodies: monoclonal mouse anti–Syt-1 antibody (antibody 41.1, catalog no. 105 011) and polyclonal rabbit anti–Syt-7 antibody (catalog no. 105 173) from Synaptic Systems. After incubation, the cells were washed five times with TBS and incubated for 70 min with Alexa-conjugated anti-rabbit and anti-mouse secondary antibodies (Molecular Probes/Invitrogen). Finally the cells were washed five times after the secondary incubation and imaged by confocal microscopy.

### Confocal microscopy

Images of immunostained endogenous Syt puncta were acquired on a Leica Biosystems TCS SP5 confocal microscope with a 63×/1.40 NA oil objective. Images of cells transfected with either Syt-1 or Syt-7 GFP were acquired on a ZEISS LSM 780 confocal microscope with a W Plan-Apochromat 63×/1.0 NA M27 water immersion objective. For imaging, a 405-nm diode laser, a 488-nm argon laser, and a HeNe red 633-nm laser were used on both the confocal microscopes. The images were analyzed with Imaris (Bitplane) software (see image analysis below). Statistical calculations where needed were performed using Prism 6 software (GraphPad Software).

### Cell stimulation

Cells were quickly washed two or three times in basal physiological salt solution (PSS) to get rid of any residual media and then used for the secretion experiments. For the total internal reflection fluorescence (TIRF) experiments, cells were perfused with PSS containing 145 mM NaCl, 5.6 mM KCl, 2.2 mM $CaCl_2$, 0.5 mM $MgCl_2$, 5.6 mM glucose, and 15 mM HEPES, pH 7.4, for 10 s and then stimulated with high-$K^+$ solution containing either 56 mM KCl (95 mM NaCl, 56 mM KCl, 5 mM $CaCl_2$, 0.5 mM $MgCl_2$, 5.6 mM glucose, and 15 mM HEPES, pH 7.4) or 25 mM KCl (126 mM NaCl, 25 mM KCl, 5 mM $CaCl_2$, 0.5 mM $MgCl_2$, 5.6 mM glucose, and 15 mM HEPES, pH 7.4) to trigger exocytosis for ∼60 s. Individual cells were perfused with a needle (100-µm inner diameter) under positive pressure applied using the ALA-VM4 perfusion system (ALA Scientific Instruments).

For repeated stimulation experiments, chromaffin cells transfected with GCaMP5G, Syt-1, or Syt-7 GFP were depolarized with elevated $K^+$ (56 mM KCl) during subsequent rounds of stimulation. The cells were initially perfused with 56 mM KCl for 30 s and then exposed to basal PSS for either 10 or 60 s to allow clearance of $Ca^{2+}$ from within the cytoplasm. After this recovery period, the cells were again exposed to elevated $K^+$ one or more times for a period of 15 s, with intermittent application of basal PSS (10 s; see Fig. 6).

### TIRF microscopy

TIRF imaging was performed on an inverted microscope (IX81; Olympus) equipped with an oil 60× objective (NA 1.49), two additional lenses (1.6× and 2×) in the emission path between the microscope, and a cooled electron-multiplying charge-coupled device camera (iXon3; Andor Technology). Two-color TIRF microscopy was performed by exciting the samples using a 488-nm argon ion laser and a 561-nm solid-state Sapphire laser (Coherent). A detailed description of this TIRF setup (along with specifics of the optical filter assembly) is provided elsewhere (Passmore et al., 2014). Lambda SC smart-shutter controllers were used for rapid switching between the excitation wavelengths (Sutter Instrument). Images were acquired with Metamorph software (Molecular Devices) successively in the green and red channels with an exposure time of 30 ms and an electron-multiplying gain of 300. The frame acquisition rate was ∼4–5 Hz for a pair of images. The final pixel size was ∼80 nm.

An Olympus cellTIRF-4Line unit was used to obtain the dual-color imaging results reported in Fig. S2. GFP and mCherry fluorescent fusion proteins were sequentially excited with 488- and 561-nm lasers. Emission was separated on an OptoSplit II system from Cairn Research. Optical filters in the OptoSplit were obtained from Semrock (FF01-514/30-25, FF02-617/73, and dichroic FF580-FDi01). A sequential pair of images were acquired at 4–5 Hz on an electron-multiplying charge-coupled device (iXon 897; Andor Technology). The final pixel size of the images was ∼80 nm. The microscope and all peripherals were controlled using Olympus CellSens software. All TIRF experiments were performed at ∼30°C.

### Determination of $[Ca^{2+}]_i$ using TIRF microscopy

We used the genetically encoded $Ca^{2+}$ indicator GCaMP5G (Akerboom et al., 2012) to determine changes in cytosolic free $Ca^{2+}$ evoked by different depolarizing solution challenges. Chromaffin cells transfected with GCaMP5G were plated on a 35-mm glass cover dish and imaged by TIRF microscopy (see "TIRF microscopy" above). The standard bath solution was a basal PSS (see "Cell stimulation" above). To depolarize the cells to evoke changes in cytosolic $Ca^{2+}$, the standard stimulating solution was adjusted to contain 5.6, 10, 25, 40, 56, 80, or 100 mM KCl while maintaining overall osmolarity of the solution. Calculations for determining the intracellular $Ca^{2+}$ concentrations were performed as described previously (Neher and Augustine, 1992; Neher, 1995; Maravall et al., 2000). A brief explanation for the same has been provided here. The mean fluores-

cence change of GCaMP5G in response to the different depolarizing stimuli was estimated as the ratio $\Delta F/F = (F - F_{base})/(F_{base})$, where F is the peak fluorescence intensity of GCaMP5G after stimulation, and $F_{base}$ is the mean fluorescence intensity in the same cell before stimulation. The averaged $\Delta F/F$ values from all KCl concentrations were used to estimate the fold change in fluorescence at GCaMP5G-$Ca^{2+}$ binding saturation (see below, $[\Delta F/F]_{plateau}$). Calcium concentrations were then calculated using the following equations (Maravall et al., 2000):

$$\frac{\Delta[Ca^{2+}]}{K_d} = \frac{F_{max}}{F_0}\left(1 - R_f^{-1}\right)\frac{\Delta F/F}{\left((\Delta F/F)_{max} - \Delta F/F\right)\cdot(\Delta F/F)_{max}},$$

where $\Delta[Ca^{2+}]$ is the rise in calcium concentration, $K_d$ is the dissociation constant (we used a $K_d$ value of 447 ± 10 nM for GCaMP5G; Chen et al., 2013), $F_{max}$ is the peak fluorescence value for each cell, $F_0$ is the mean baseline fluorescence before stimulation for each cell, $R_f$ is the dynamic range of the indicator (we used an $R_f$ value of 45.4 ± 0.9 for GCaMP5G; Chen et al., 2013), $\Delta F/F$ is the change in fluorescence divided by the baseline fluorescence, $(\Delta F/F)_{max}$ is the corrected $\Delta F/F$ at saturation (see below), and $(\Delta F/F)_{max}$ was calculated on the basis of the equation below. Saturation of GCaMP5G occurred at 80 and 100 mM KCl (see Fig. 7 A), and these values were used to determine the correction factor, x:

$$(\Delta F/F)_{max} = (\Delta F/F)_{plateau} * 100/x,$$

where x is a correction factor:

$$x = 100 * \frac{1 - Q*\left(\frac{\upsilon_1}{\upsilon_2}\right)}{1 - (\upsilon_1/\upsilon_2)},$$

where υ1 and υ2 are the lower and higher KCl concentrations driving stimulation (80 and 100 mM) at GCaMP5G saturation, and Q is the ratio of plateau fluorescence at higher and lower KCl stimulus (Maravall et al., 2000).

The mean resting calcium concentration ($[Ca^{2+}]_0$) within control unstimulated cells was determined using the following equation (Maravall et al., 2000):

$$\frac{[Ca^{2+}]_0}{K_d} = \frac{1 - R_f^{-1}}{(\Delta F/F)_{max}} - R_f^{-1},$$

### Ratiometric $Ca^{2+}$ imaging for determination of intracellular $[Ca^{2+}]$

We used the ratiometric $Ca^{2+}$ indicator fura-2 (TEFLabs) to determine changes in cytosolic free $Ca^{2+}$ evoked by different depolarizing solution challenges. Cells cultured on glass coverslips were used to form the bottom of a recording chamber and loaded at room temperature for 45 min with 2 µM fura-2 AM in physiological saline. Local application of bath or stimulus solutions through small-bore glass capillary tubing was achieved using a pressure-driven reservoir. The standard bath solution was a basal PSS (see "Cell stimulation" above). To depolarize the cells to evoke changes in cytosolic $Ca^{2+}$, the standard bath solution was adjusted to contain 10, 25, or 56 mM KCl while maintaining overall osmolarity of the solution. Dye fluorescence was monitored using a monochromator-based digital imaging system (T.I.L.L.-Photonics) coupled to a Nikon TE-2000 microscope. Cells were alternately excited at 340/380 ± 15 nm reflected onto the plane of focus using a DM400 dichroic mirror and Super Fluor 40×, 1.3 NA oil immersion objective. The emitted fluorescence was collected through a 510 ± 25 nm band-pass filter (Chroma Technology Corp.).

For dye calibration, we used the in vivo procedure in which the calibration constant values for $R_{min}$, $R_{max}$, and $K_{eff}$ were determined from three to five cells dialyzed through patch pipette with standard internal recording solution adjusted to contain either minimal $Ca^{2+}$ (10 mM EGTA, no added $Ca^{2+}$) or saturating $Ca^{2+}$ (3 mM $Ca^{2+}$) concentrations and containing 150 µM fura-2 (Giovannucci and Stuenkel, 1997). Values for $R_{min}$, $R_{max}$, and $K_{eff}$ were 0.44, 5.52 and 972 nM, respectively.

### Digitonin permeabilization experiments

Permeabilized chromaffin cell experiments were performed as described elsewhere (Bittner and Holz, 1992). First the nutrient media were washed off the dish and replaced with sodium glutamate solution (NaGEP) containing 139 mM sodium glutamate, 20 mM PIPES, 2 mM MgATP, and 0.2 mM EGTA, pH 6.6, with no added $Ca^{2+}$. The EGTA in the bath solution helps control the levels of free calcium in a precise and reproducible manner. To extend the range of concentrations tested above 30 µM, nitrilotriacetic acid was used in place of EGTA to chelate $Ca^{2+}$. Individual cells were then perfused with NaGEP solution (0.2 mM EGTA) for 10 s and then permeabilized by switching to NaGEP solution (5 mM EGTA) containing 40 µM digitonin for 50 s with varying concentrations of free $Ca^{2+}$ (1, 5, 10, 30, and 100 µM). The amount of free $Ca^{2+}$ in the solution was calculated using the Martell and Smith constants for EGTA-$Ca^{2+}$ binding. A stock NaGEP solution with 30 µM free $Ca^{2+}$ was made using 4.693 mM $CaCl_2$ (total $Ca^{2+}$). Other concentrations of $Ca^{2+}$ were made by mixing the $Ca^{2+}$-free and the 30-µM $Ca^{2+}$ stock solutions together in the appropriate ratios. NaGEP solution with 100 µM free $Ca^{2+}$ was also made using 4.97 mM $CaCl_2$ (total $Ca^{2+}$).

### Channel blocker experiments

Stock solution of nifedipine (L-type; Sigma-Aldrich) was prepared in DMSO at a concentration of 10 mM

and diluted with the bath solution (PSS; see "Cell stimulation") to the required final concentration of 3 µM. ω-Conotoxin GVIA (N-type) and ω-conotoxin MVIIC (N/P/Q-type; Sigma-Aldrich) were prepared in distilled water to a stock concentration of 1 mg/ml and kept in aliquots at −20°C until use. ω-Conotoxin GVIA and ω-conotoxin MVIIC were used at final concentrations of 1 and 3 µM in PSS, respectively. Chromaffin cells transfected separately with GCaMP5G, Syt-1, or Syt-7 GFP were incubated with the above-listed $Ca^{2+}$ channel blockers alone or in combination. The effect of channel blockers was then determined using TIRF microscopy after stimulation of exocytosis with 56 mM KCl. The control cells were imaged before application of the blockers. The percentage reduction in exocytosis is based on the difference in the number of fusion events between control and treated cells.

### Image analysis: Identification of exocytotic sites

The images obtained from confocal microscopy were analyzed using a software-based approach with Imaris using the "spot function" module for object-based colocalization analysis. To determining the distance of the Syt granules from the nearest point on the cell surface, confocal z-sections were used to render a 3D surface in Imaris. The Syt GFP granules within the evanescent field were tracked using a custom script (Degtyar et al., 2007) developed in IDL (ITT).

The images obtained from TIRF microscopy were analyzed in multiple ways. Determination of Syt GFP fusion events were identified primarily on the basis of the increase in fluorescence after fusion with the plasma membrane (see explanation below). We selected events on the basis of a minimum 20% increase in GFP fluorescence after fusion. In some cases, the initial rise in fluorescence was followed by a decrease as Syt GFP diffuses along the plasma membrane. Fusion of GFP containing granules with the plasma membrane results in brightening of fluorescence for two reasons: (1) GFP (pKa 5.9) present within the granule lumen encounters the neutral pH (7.4) of the extracellular medium, causing slight dequenching of the fluorophore, and (2) the increased strength of the evanescent field at the plasma membrane–coverslip interface causes greater excitation of the GFP molecules (Kneen et al., 1998; Tsien, 1998; Campbell and Choy, 2001).

The Syt-1 pHluorin/Syt-7 pHuji emission images were captured sequentially using Metamorph software. Individual granules undergoing exocytosis were evident by an increase in the pHluorin/pHuji intensity after fusion with the plasma membrane because of the change in pH of the granule. The changes in the fluorescence intensity over time for the different fusion events were calculated after normalization for every fusion event using custom software written in IDL.

### Image analysis: Clustering

The possible tendency of exocytotic sites to cluster in localized regions was examined by quantitatively analyzing the distribution of exocytotic sites in comparison with random positions as generated by a computer. This was done with a custom program written in IDL, with a multistep protocol that built on algorithms written for a previous study (Allersma et al., 2004). On a stack of sequential experimental images, the (x,y) positions of exocytotic events are located by eye as sudden increases in local fluorescence. These locations are recorded by mouse click without regard to which frame the event occurred during. The total number of selected events is recorded. Then, the distance $r = (x^2 + y^2)^{1/2}$ between every pair of events is calculated and grouped in bins of range $n\Delta r$ to $(n + 1)\Delta r$, where $\Delta r$ is a user-settable width of each bin, and n is an integer ranging from zero to some maximum value such that the maximum $(n + 1)\Delta r$ is larger than the maximum dimension of a cell. The number of events that fall into each bin, plotted against the radius of each bin, is the pairwise distance histogram of the experimental exocytotic events.

That experimental histogram must be compared with the histogram expected from a random distribution of simulated event locations. The simulated histogram can be generated by assigning locations independently to x and y with a random number generator. It is essential, however, that randomly selected (x,y) locations be accepted only if they fall within the perimeter of the cell footprint (which must be outlined in the operation of the software program). Any other (x,y) position must be rejected. The generation of successful locations continues until there are exactly the same number of simulated events as was seen in the experimental data. Then, a histogram for simulated random positions is generated exactly the same way as for experimental data. Because each simulation produces a different scatter of event locations, the simulation procedure can be repeated very quickly as often as necessary to gain a good estimate of the mean and SD of the simulated histograms. A set of "difference histograms" ($H_D$ vs. r) can be produced, showing the difference between the actual experimental histogram and each simulated histogram. The set of $H_D$ versus r histograms has the same SD as the simulated histograms themselves. If $H_D$ falls within an SD of zero, then the experimental event distribution is not distinguishable from a random distribution. If $H_D$ versus r is at least several SDs different from zero for at least some radii, then the experimental distribution cannot be random. Depending on which range of radii shows $H_D$ significantly greater than zero allows us to conclude that whether the actual events are clustered ($H_D > 0$ for small radii) or anticlustered ($H_D > 0$ for large radii).

### Online supplemental material

Fig. S1 shows quantitation of intracellular $Ca^{2+}$ levels in depolarized chromaffin cells using TIRF microscopy and epifluorescence imaging techniques. Fig. S2 shows dual-color imaging experiments performed to determine mobility and fusion efficacy of granules harboring NPY mCherry and either Syt-1 or Syt-7 GFP. Fig. S3 shows the stimulation dependence of exocytosis from docked and newcomer Syt-1 or Syt-7 granule populations. Fig. S4 shows analysis of the intracellular distribution of granules harboring Syt-1 or Syt-7. Fig. S5 shows the effects of repeated stimulation on the near-membrane levels of $Ca^{2+}$using gCaMP5G as a molecular indicator.

## RESULTS

### Distinct fusion kinetics of Syt-1– and Syt-7–bearing granules

Chromaffin cells granules have traditionally been segregated into "pools" defined by their fusion kinetics (measured by increases in membrane capacitance) in response to electrophysiological stimulation (Voets et al., 1999; Voets, 2000; Sørensen, 2004). We sought to approximate this approach using a combination of chemical stimulation and TIRF imaging of individual Syt fusion events. Our initial purpose was to determine if there were differences in activation kinetics of individual granules that could be attributed specifically to the presence of Syt-1 and Syt-7 on the granule membrane. We previously reported that Syt isoforms show little to no colocalization on granules, even when overexpressed as fluorescent fusion proteins (Rao et al., 2014). To assay for differences in fusion kinetics, we cotransfected plasmids encoding Syt-1 pHluorin and Syt-7 pHuji (Shen et al., 2014) so that both isoforms could be observed and their respective time courses of fusion precisely known. Cells expressing fluorescent Syts were identified after a brief incubation with $NH_4Cl$ (Fernández-Alfonso et al., 2006; Rao et al., 2014) and subsequently depolarized with 25, 56, or 80 mM KCl for 40 s. There were only a handful of fusion events for Syt-1 with 25 mM KCl, but at both 56 and 80 mM depolarization, the number of fusion events was sufficiently large for us to evaluate fusion kinetics.

We observed that Syt-7 granules fused earlier than Syt-1 after depolarization with elevated KCl (Fig. 1, A–C). This can be seen in the representative images and traces of Syt-1 and Syt-7 events from a single cotransfected cell, where Syt-7 pHuji events begin almost immediately after application of 56 or 80 mM KCl (Fig. 1 B). Syt-1 events follow after a brief but measurable delay. We also compared the frequency distribution of all fusion events on the basis of the time at which they occurred after depolarization (Fig. 1 C). The events were binned into 1-s intervals and fit with a Gaussian for 56 mM KCl and 80 mM KCl. Notably, the mean for Syt-7 events was shifted to shorter times at both 56- and 80-mM stimulation conditions (7.01 and 6.10 s, respectively), in relation to Syt-1 events in the same cells (8.86 and 8.11 s, respectively).

Depolarization with high extracellular KCl drives exocytosis by elevating intracellular $Ca^{2+}$ near fusion sites. But how comparable is the $Ca^{2+}$ increase with KCl depolarization to what might be measured after electrophysiological depolarization? To answer this question, we quantitated $Ca^{2+}$ levels in the evanescent field using the fluorescent $Ca^{2+}$-binding protein GCaMP5G (Akerboom et al., 2012). GCaMP5G fluorescence increases upon $Ca^{2+}$ binding, and this increase can be represented as a fold change ($\Delta F/F$) in fluorescence intensity (Fig. S1 A). Binding of GCaMP5G to $Ca^{2+}$ was saturated upon application of stronger KCl solutions ($\geq$56 mM). Using this information, we were able to approximate the total internal $Ca^{2+}$ concentration ($[Ca^{2+}]_i$) resulting from application of each KCl solution on the basis of the equations described in Materials and methods (Maravall et al., 2000). We observed that the rise in total internal $Ca^{2+}$ was directly related to the concentration of KCl used to depolarize the cell (Fig. S1 B). Even with the strongest depolarization (100 mM KCl), the $[Ca^{2+}]$ saturates at ~5 µM. This is likely in the lower range of what has been reported for $Ca^{2+}$ near fusion sites after electrophysiological depolarization of chromaffin cells (Augustine and Neher, 1992). We also measured intracellular $Ca^{2+}$ changes using the ratiometric $Ca^{2+}$ indicator fura-2 and observed a similar concentration-dependent change in $[Ca^{2+}]_i$ levels on the basis of the strength of the KCl solution (Fig. S1 C; Neher, 1995; Giovannucci and Stuenkel, 1997).

$Ca^{2+}$ ostensibly enters cells through voltage-gated channels upon membrane depolarization. To verify that the source of $Ca^{2+}$ for exocytosis was extracellular, we incubated chromaffin cells expressing GCaMP5G with $Ca^{2+}$ channel blockers nifedipine (L-type), ω-conotoxin GVIA (N-type), and ω-conotoxin MVIIC (N/P/Q-type; Hernández-Guijo et al., 1998). Each blocker applied alone significantly reduced the influx of $Ca^{2+}$ upon membrane depolarization. When the blockers were applied together, increases in $Ca^{2+}$ fluorescence were almost completely absent (Fig. 2 A).

As one might expect, inhibition of $Ca^{2+}$ channel activity also had downstream effects on $Ca^{2+}$-triggered exocytosis. Interestingly, subtype-selective channel blockade differentially inhibited fusion in Syt-1 and Syt-7 granules with respect to both degree (Fig. 2 B) and kinetics (Fig. 2, C–E) of fusion. For example, all the blockers significantly reduced the fusion probability of Syt-1 GFP. But the application of nifedipine had almost no effect on Syt-7 granule fusion and, unsurprisingly, also had no effect on shifting Syt-7 fusion kinetics. In both groups, fusion kinetics were most significantly slowed after ap-

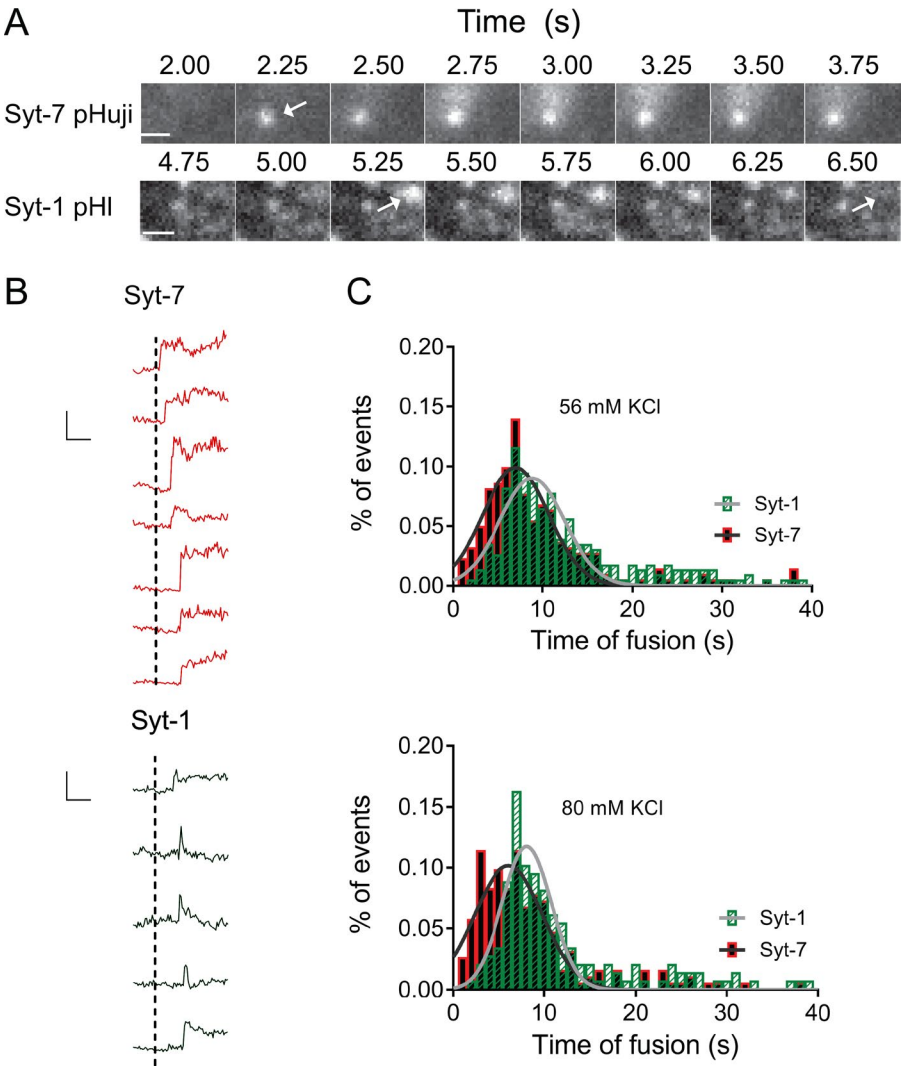


Figure 1. **Fusion kinetics of Syt isoforms after KCl depolarization.** Syt-1 pHluorin (pHl) and Syt-7 pHuji were coexpressed simultaneously in the same chromaffin cell, and exocytosis was triggered by stimulation with KCl of different concentrations (56 and 80 mM). (A) Representative fusion events for Syt-1 pHl and Syt-7 pHuji granules. Fusing granules are indicated by arrows. Time 0 s (not depicted) represents the start of stimulation. Bars, 800 nm. (B) Representative traces for Syt-1 pHl and Syt-7 pHuji fusion events from the same cell all aligned to the start of the stimulation period (dotted line). Syt-7 pHuji granules begin fusing before Syt-1 pHl granules after stimulation. Bar, 200 A.F.U. and 5 s. (C) Frequency distribution of all fusion events after depolarization with 56 mM KCl (top; Syt-1 pHl, 402 events; Syt-7 pHuji, 226 events; $n$ = 11 cells) and 80 mM KCl (bottom; Syt-1 pHl, 211 events; Syt-7 pHuji, 197 events; $n$ = 8 cells) binned into 1-s intervals. The data were fit with a Gaussian to determine the mean time of fusion for Syt-1 pHl (8.86 s at 56 mM and 8.11 s at 80 mM) and Syt-7 pHuji (7.01 s at 56 mM and 6.10 s at 80 mM) events upon stimulation with KCl. Differences between Syt-1 and Syt-7 mean fusion times at 56 and 80 mM were statistically significant ($P < 0.0001$).

plication of MVIIC (see dotted lines shifted to the right of the solid lines).

### Syt-7 has a greater tendency to fuse in "clusters" than Syt-1

The above results suggest that Syt-1 and Syt-7 granules are likely to be differentially dependent on $Ca^{2+}$ channel subtypes for exocytosis. To look more directly at spatial heterogeneity in granule fusion sites, we mapped fusion sites of Syt-1 and Syt-7 granules on the chromaffin cell footprint. We used an automated procedure (custom written in IDL) to determine distances between every pair of fusion locations (Fig. 3). The program compares the experimental distances with those obtained from the same number of spots placed at random within a hypothetical cell of the same size and shape footprint. The number of times a particular distance r between fusion locations occurs is plotted on the ordinate axis, while the actual r-distance (in pixels; 1 pixel = 80 nm) is plotted on the abscissa. In this way, several histograms are formed for each cell: one histogram for the actual experimental fusion locations and a whole set of histograms for the repeated sets of random fusion placements. Cartoons of an actual chromaffin cell fusion location set and footprint are shown in Fig. 3 (A and B). Fig. 3 A shows the distribution of Syt-1 GFP fusion locations, whereas Fig. 3 B shows the distribution of Syt-7 pHuji fusion locations.

From the numerous histograms generated from simulated random event locations (typically 50), a reliable SD can be established for simulated histograms within each r-distance bin. After analysis, it is evident that the experimental histogram for Syt-7 fusion events (Fig. 3 D) does not overlap much with the set of histograms generated from hypothetical random locations. In fact, the occurrence of experimental Syt-7 granule fusion events separated by 57 pixels is roughly 70% higher than what would be expected if the events occurred at random locations. A "difference histogram" $H_D$ versus r between the experimental histogram and each of the simulated histograms can be established and plotted (Fig. 3 E for Syt-1 and Fig. 3 F for Syt-7).

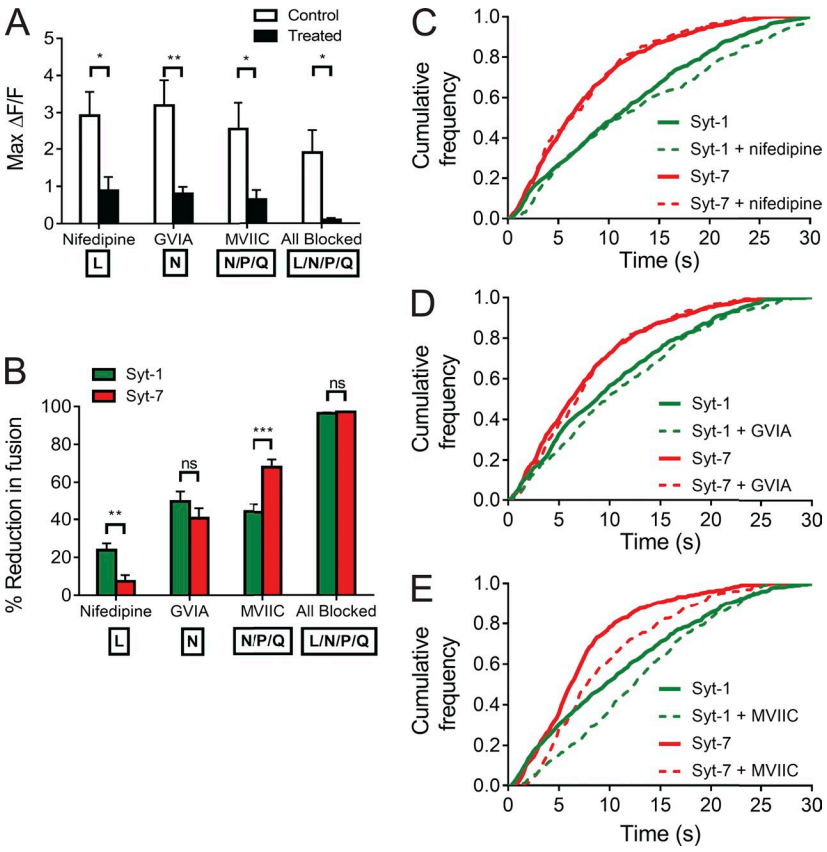


Figure 2. **Effect of $Ca^{2+}$ channel blockers on granule fusion.** (A and B) Chromaffin cells were transfected separately with GCaMP5G (A) or Syt-1 or Syt-7 GFP (B) and exposed to different $Ca^{2+}$ channel blockers at the following concentrations: nifedipine (L-type blocker) 3 µM, ω-conotoxin GVIA (N-type blocker) 1 µM, ω-conotoxin MVIIC (N/P/Q-type blocker) 3 µM, or all three blockers together. The cells were stimulated with 56 mM KCl after a 10-min incubation with the listed blockers. For A, the graph shows the averaged maximal fold changes in GCaMP5G fluorescence (ΔF/F) mean depolarization. Error bars depict SEM ($n$ = 5 cells for all conditions). Statistical differences were assessed using Student's $t$ test (*, $P < 0.05$; **, $P < 0.01$). For B, the percentage reduction is based on the difference between fusion events in control and treated cells (Fig. S3 B; $n$ = 18 cells for all conditions except "all blocked," for which $n$ = 6 cells). Statistical differences were assessed using Student's $t$ test (**, $P < 0.01$; ***, $P < 0.001$). (C–E) Changes in fusion kinetics for Syt-1 or Syt-7 GFP granules with the indicated blocker are shown. When blocked with nifedipine or GVIA, the change in kinetics is not significant between the treated and control groups (Mann-Whitney test, ns, $P > 0.05$). However, for MVIIC, the change in kinetics with blocker (dotted line) is significant (Mann-Whitney test, $P < 0.01$, $n$ = 12 cells for all conditions).

The $H_D$ versus r curves have a spread given by the SD of the simulated histograms and should be significantly different from zero at any r only if the experimental events are clustered or anticlustered. The difference histograms of Fig. 3 (E and F) can be replotted to show the number of SDs by which they depart from zero, thereby showing the statistical significance of the experimental data's departure from the mean of the simulations (Fig. 3, G and H). For many of the individual Syt-7 cells, $H_D$ versus r is significantly greater than zero at smaller r-distances, by six deviations, showing the fusion locations tend to be closer together than would be expected from random placement. Averaging these difference histograms over all the Syt-7 cells (Fig. 3 J) still clearly shows a significant tendency toward clustering. On the other hand, the Syt-1 fusion event histograms and the random histograms are largely indistinguishable (Fig. 3, G and I). This analysis shows that Syt-1 fusion locations are randomly dispersed, and Syt-7 fusion locations are clustered.

### Syt-1 granules are more mobile than Syt-7 granules

We next asked whether granules bearing either Syt-1 or Syt-7 demonstrated differences in mobility. If some subset of granules (e.g., Syt-1) must travel a greater distance before fusion, fusion kinetics are likely to be delayed as a consequence (Fig. 1). Although z-direction movements of granules could not be reliably measured, movements of granules in x and y within the TIRF evanescent field can be readily observed and quantitated. To perform these studies, Syt-1 or Syt-7 was expressed in cells as GFP fusion proteins and tracked for tens of seconds during membrane depolarization with 56 mM KCl. First, the mobility of all granules within the evanescent field was measured, irrespective of whether they would eventually fuse. An example of a Syt-1 cell's granule tracks is shown in Fig. 4 A. We found that docked Syt-1 granules exhibited more movement on average than docked Syt-7 granules (100 ± 12 nm from a start position to end position for Syt-1, compared with a mean of 63 ± 7.8 nm for Syt-7; Fig. 4 B). The mean x and y velocities of granules harboring Syt-1 or Syt-7 isoforms were also measured. The velocities were small, consistent with the relative overall lack of granule movement (Fig. 4, C and D).

Next, we considered only the mobility of those granules destined to fuse. Before stimulation, both Syt-1 and Syt-7 granules undergo small x and y (R) motions in the plane of the cell membrane. It is clear from monitoring these motions that granules tend to fuse at sites that are tens to hundreds of nanometers displaced from their initial positions at the start of stimulation (Fig. 5 A, solid circle). Granules were tracked within the evanescent field using a custom script developed in IDL (Degtyar et al., 2007). Representative tracks for Syt-1 and Syt-7 granules in the seconds before fusion are shown in Fig. 5 B.

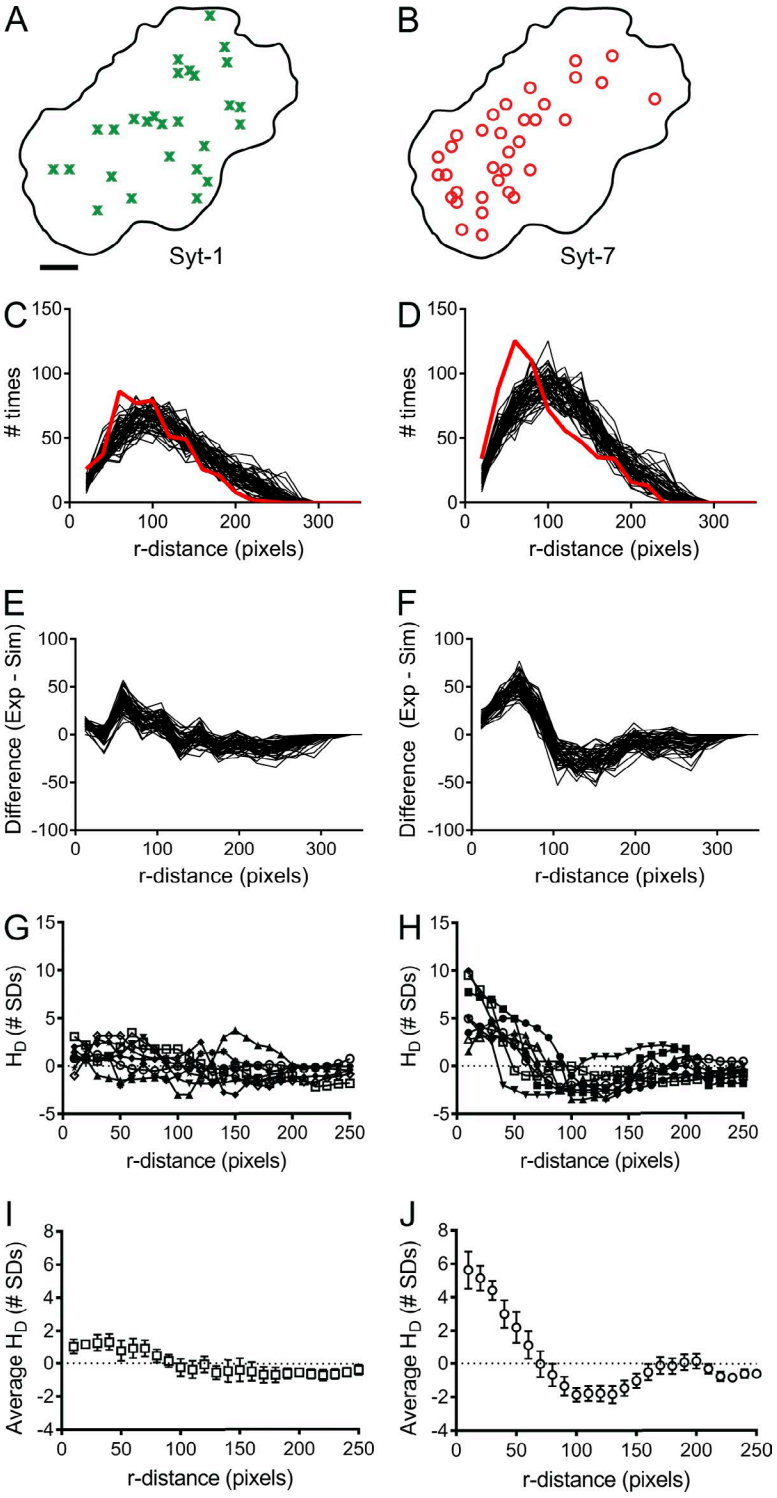


Figure 3. **Mapping and cluster analysis of Syt-1 and Syt-7 fusion events.** (A and B) Outlines of a particular chromaffin cell footprint. Fusion locations of Syt-1 GFP (green x's) and Syt-7 pHuji (red circles) granules are indicated. Bar, 42 pixels (80 nm/pixel). (C and D) For the cell in A and B, fusion event histograms for 50 simulated locations (chosen at random, black lines) and experimental locations (green line, Syt-1; red line, Syt-7) are shown, with r-distances grouped into bins of 10 pixels each. Whereas the Syt-1 experimental and random event histograms are mostly overlapping, the Syt-7 experimental and random event histograms are clearly distinguishable. (E and F) Difference histograms ($H_D$) between the experimental histogram of C and D, respectively, and each of 50 simulated histograms are plotted. (G and H) Difference histograms replotted in units of the number of SDs by which experimental data differ from simulated data, versus separation distance, r. The difference histograms for each of eight different cells expressing Syt-1 and Syt-7 are shown. The graphs use different symbols for each cell. (I and J) Difference histograms for the graphs shown in G and H, here averaged over the eight cells with standard error bars shown. The averaged Syt-1 and Syt-7 histograms are significantly different at 10, 20, and 30 pixels ($P < 0.001$) and 90, 100, and 120 pixels ($P < 0.05$).

The red X indicates the site of fusion. We quantified this motion by taking the frame-by-frame, poststimulation ΔR expressed relative to its ΔR before stimulation. This normalization was necessary because it was apparent that certain granules are inherently more mobile than others. Fig. 5 C shows the mean ΔR (poststimulation)/ΔR (prestimulation) for fusing Syt-1 and Syt-7 granules. In the moments leading to fusion, Syt-1 and Syt-7 mobility is similar. However, in the last 200 ms before fusion, Syt-1 granules tend to travel greater distances than Syt-7 granules. The sudden increased motion is specific to fusing granules. For example, when the motion of nonfusing granules (typically within 2–5 granule diameters of fusing granules) was tracked alongside their fusing neighbors, there was no measurable increase in movement (not depicted). The displacement of individual

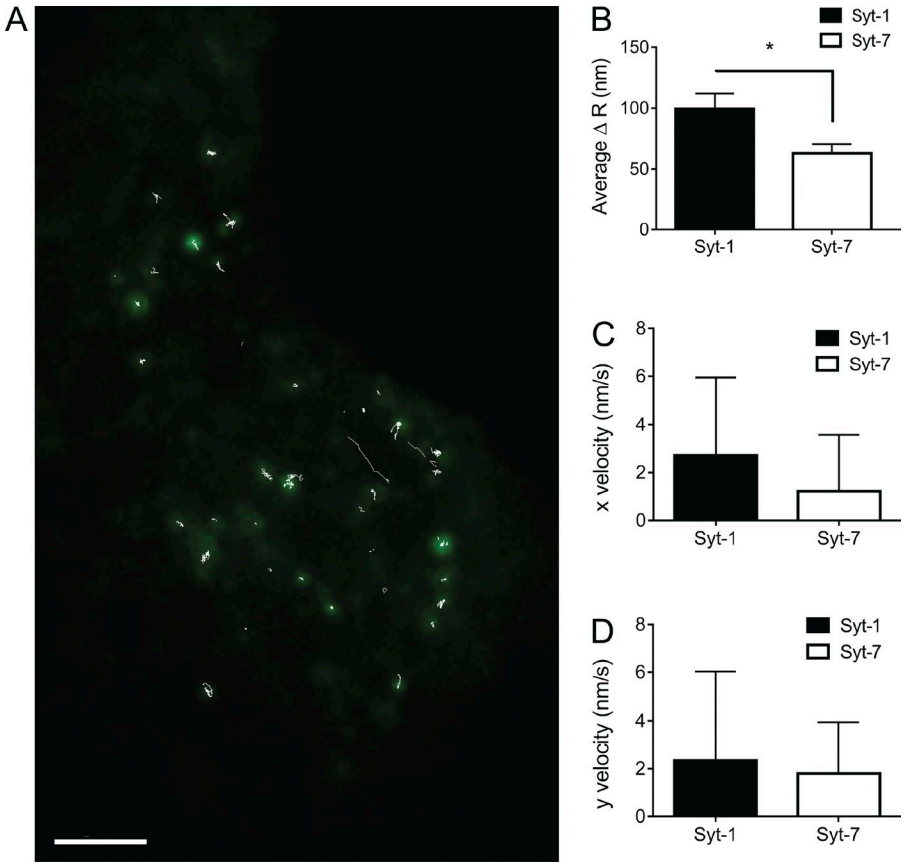


Figure 4. **Mobility of all docked Syt-1 and Syt-7 granules.** (A) A chromaffin cell stimulated with 56 mM KCl and expressing Syt-1 GFP. Granule tracks which are at least 10 s in duration are indicated in white. Bar, 4 µm. (B) The mean displacement (Δ R) of Syt-1 and Syt-7 GFP labeled granules. Error bars represent SEM. Differences between the Syt-1 and Syt-7 granule populations were assessed using Student's *t* test ($n$ = 6 cells, 582 tracks Syt-1; $n$ = 5 cells, 322 tracks Syt-7; *, $P < 0.05$). (C and D) Mean x and y velocities of Syt-1 GFP or Syt-7 GFP granules. Error bars represent SEM. The difference in velocities was not statistically different (ns, $P > 0.05$).

Syt-1 and Syt-7 granules from the start position to the fusion site was also measured (Fig. 5 D). Again, we found that Syt-7 granules tend to travel a shorter distance to fusion sites, on average, than Syt-1 granules.

We validated these results with two-color imaging experiments in which both NPY mCherry and Syt GFP were expressed in chromaffin cells (Fig. S2 A). The NPY mCherry allowed us to know unambiguously that a Syt-bearing granule had actually fused and released its contents (Fig. S2, C–E). Syt and NPY exhibited a colocalization frequency of ~20%, irrespective of the isoform expressed (Fig. S2 B). The mobility of specifically those Syt granules destined for fusion and colabeled with NPY Cherry were tracked (Fig. S2 G). Qualitatively, these results are similar to those shown in Fig. 5 D. Although both Syt-1 and Syt-7 granules exhibited more motion just before fusion, movement was greater for Syt-1 granules than for Syt-7 granules.

### Newcomers constitute a greater proportion of Syt-1 granule fusion events than Syt-7 granule fusion events

The previous studies showed that chromaffin granules exhibit relatively small x and y motions in the plane of the membrane before fusion. However, a minority of fusion events result from granules not initially present in the evanescent field before stimulation. Instead, these granules move to the plasma membrane from deeper within the cell during depolarization. We initially observed "newcomer" fusion events in granules harboring NPY GFP (Fig. S3 A). Interestingly, there is a greater tendency for newcomer fusion events to occur the more strongly a cell is depolarized (Fig. S3 A).

We thus asked whether Syt-1 or Syt-7 granule fusion is more likely to occur with newcomers. An example of a Syt-1 fusion event from a granule not initially in the evanescent field at the start of imaging is shown in Fig. 6 A. The granule moves into the field by 5 s after stimulation and fuses at 14.4 s after stimulation. When many cells are analyzed, it is evident that newcomers constitute a greater proportion of the total number of Syt-1 fusion events than do Syt-7 newcomers for Syt-7 events (Fig. 6 C). We also found that the likelihood of a newcomer Syt-1 granule fusing (73.9% with 56 mM KCl) is greater than the likelihood of a newcomer Syt-7 granule fusing (64.5% with 56 mM KCl). In both cases, the fusion probability is already quite high compared with the fusion probability for docked vesicles (Fig. 7). The time course of newcomer fusion shows a similar trend for both isoforms, with a greater number of newcomers fusing later in the stimulus (Fig. 6 D). Over time, as the docked pool is depleted and the membrane potential remains depolarized, additional granules from within the cell are progressively recruited for fusion.

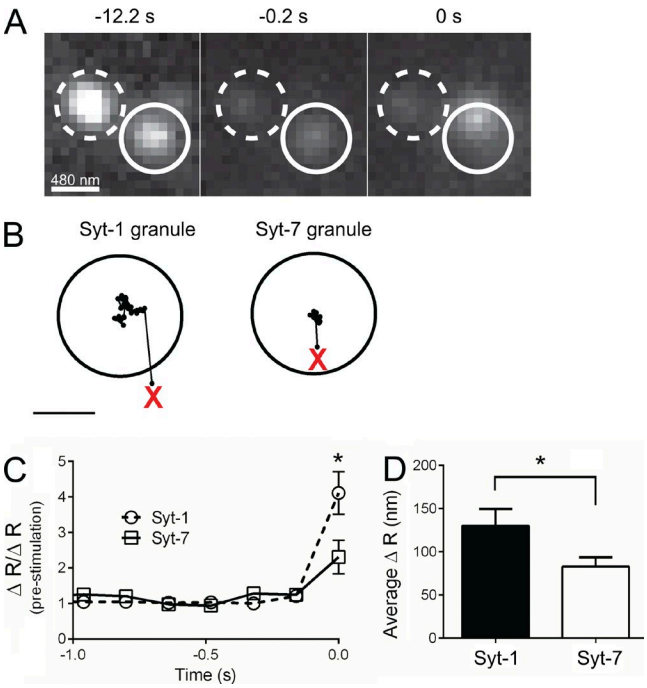


Figure 5. **Mobility of fusing Syt-1 and Syt-7 granules.** (A) Images of fusing (solid circle) and nonfusing (dashed circle) Syt-1 GFP granules at the start of stimulation (−12.2 s), immediately before fusion (−0.2 s), and at fusion (0 s). The nonfusing granule remains within the dashed circle even after 12.2 s of stimulation as seen at time 0. Its fluorescence dims as a result of processes unrelated to fusion (movement in z and photobleaching). The fusing granule significantly increases its x, y motion in the frame immediately before fusion. Note displacement of the fluorescent punctum within the solid circle between −0.2 and 0 s. Bar, 480 nm. (B) Representative frame-to-frame tracks for Syt-1 and Syt-7 GFP during the 3 s before fusion (Red X) after stimulation with 56 mM KCl. Bar, 150 nm. (C) Mean frame-to-frame motion of fusing Syt-1 and Syt-7 granules in the 1 s before fusion (time 0). Statistical differences were assessed by the Student's *t* test ($n$ = 6 cells, 23 tracks, Syt-1; $n$ = 5 cells, 24 tracks, Syt-7; *, $P < 0.05$). (D) Mean displacement of Syt-1 and Syt-7 granules from the start position to the fusion position in B. Statistical differences were assessed using Student's *t* test (*, $P < 0.05$). Error bars represent SEM.

Because a greater proportion of Syt-1 fusion events result from newcomers, we sought to identify whether there were differences in Syt granule distribution. Such differences may suggest preferential sorting to a docked or, conversely, more mobile pool found deeper within the cell. We thus used confocal microscopy to directly measure distances of fluorescent granules from a cell surface. We first analyzed the distribution of endogenous Syt within chromaffin cells using commercially available isoform-specific antibodies. After identifying fluorescent Syt puncta, confocal z-sections (0.71 µm) were used to render a 3D surface representing the approximate contours of the plasma membrane (Fig. S4 A). The images showed Syt-1 and Syt-7 puncta to share a roughly overlapping distribution, with small but significant differences in their respective distance from cell surface (Fig. S4 C). We repeated the analysis in cells overexpressing Syt-1 or Syt-7 GFP and stained with the carbocyanine dye diD. Again, the distances measured between the respective Syts and the fluorescent surface membrane were significantly different (Fig. S4, D and E).

### Syt granules differ in their responses to repeated stimulation

Granule population "releasability" has typically been defined by curve fitting to exponential components of a membrane capacitance increase (Voets, 2000; Sørensen, 2004). The "mature" or "readily releasable" pool of granules, which fuses with fast kinetics, may be the first to be depleted after depolarization. Conversely, granules that fuse more slowly with respect to the start of stimulation ("slowly releasable pool") may undergo changes that allow them to be mobilized and transition to a "fusion-ready" state. We reasoned that using TIRF microscopy, it may be possible to identify differences in releasability of granule pools by measuring differences in fusion kinetics and probability in response to elevated KCl depolarization.

Chromaffin cells expressing either Syt-1 or Syt-7 GFP were depolarized with repeated pulses of 56 mM KCl and 80 mM KCl, as shown in Fig. 7. We then calculated the percentage of docked Syt-1 and Syt-7 granules that underwent fusion. We sought to determine whether one population of granules was depleted more readily than the other, particularly at later time points in the stimulation cycle. When cells were depolarized with 56 mM KCl, the percentage of docked Syt-1 granules that fused is higher than it is for Syt-7 granules at every time point (Fig. 7 A). With 80 mM KCl, the percentage of docked Syt-1 granules fusing is higher for the second and third time points (Fig. 7 B). Interestingly, when we extended the interstimulus interval from 10 s to 60 s (the stimulation protocol was otherwise identical) fusion occurred with equal probability in both populations (Fig. 7, C and D).

We also visualized intracellular $Ca^{2+}$ during the stimulus protocol to determine whether it continued to accumulate with time or whether it effectively recovered to baseline levels in the subplasmalemma between stimulus applications. Indeed, high amounts of residual $Ca^{2+}$ between stimulus applications might exaggerate the level of Syt-7 granule fusion given this isoform's higher $Ca^{2+}$ affinity. For that reason, we monitored intracellular $Ca^{2+}$ with the genetically encoded $Ca^{2+}$ indicator GCaMP5G in cells subjected to multiple rounds of depolarization with 56 mM KCl as before (Fig. S5). The data show that depolarization-induced elevations in intracellular $Ca^{2+}$ do largely recover to baseline, but not completely. Even this relatively small level of $Ca^{2+}$ may be enough to elevate Syt-7 granule fu-

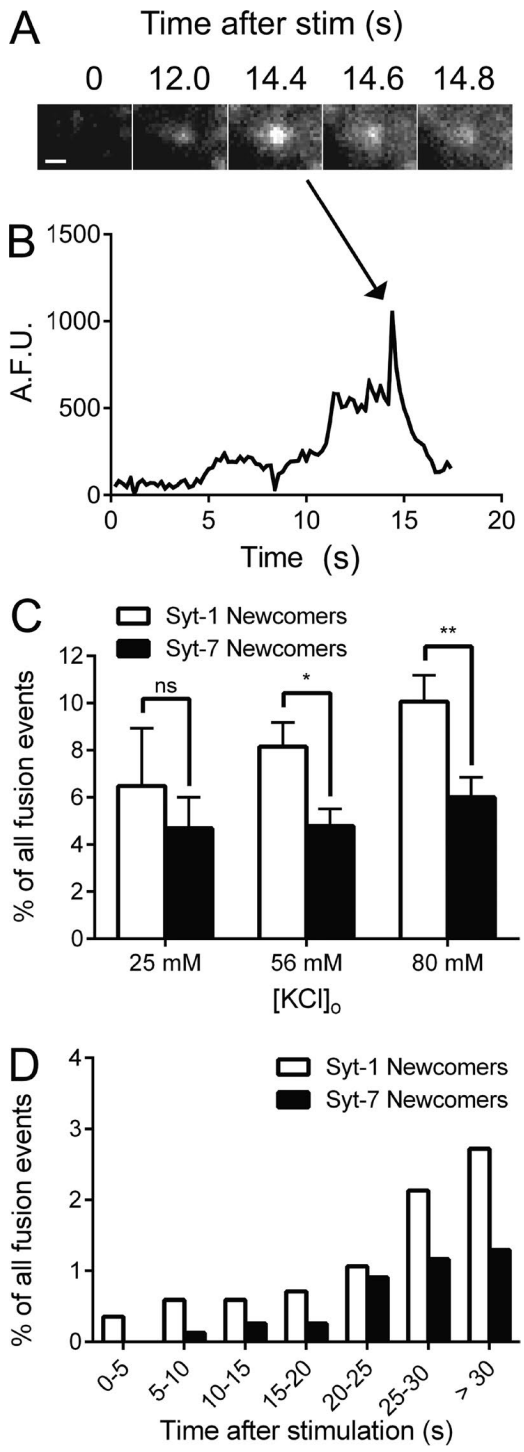


Figure 6. **The fusion properties of newcomer granules.** Syt-1 or Syt-7 GFP was expressed separately in chromaffin cells, and exocytosis was triggered by stimulation with KCl. (A) An example of a Syt-1 GFP newcomer fusion event. The granule appears in the evanescent field ~5 s after the depolarization and fuses at 14.4 s after depolarization. Bar, 800 nm. (B) Intensity versus time graph for event in A. The arrow indicates the rise in intensity corresponding to the fusion event. (C) Bar graph depicts the percentage of newcomer granules that fuse in relation to the total number of fusion events ($n$ = 12 cells [25 and 80 mM KCl], $n$ = 18 cells [56 mM KCl]). Statistical differences were assessed using Student's $t$ test (*, $P < 0.05$; **, $P < 0.01$). Error bars represent SEM. (D) Time course for newcomer Syt-1 and Syt-7 fusion events after stimulation with 56 mM KCl ($n$ = 18 cells). The percentage of newcomer events is based on the total number of fusion events and binned into 5-s intervals. Note that there is a greater proportion of Syt-1 newcomer fusion events in comparison with Syt-7 newcomer fusion events at all time points.

sion probability to levels that are near Syt-1 at stimulus cycles 2 and 3.

### Chromaffin granules fuse at different rates and efficacies in response to $Ca^{2+}$

Both Syt-1 and Syt-7 granules fuse with high efficacy when cells are depolarized with 56 or 80 mM KCl (Figs. S2 F and S3 B). At depolarization intensities that are more modest, as with 25 mM KCl, Syt-7 granules fuse with greater efficacy than Syt-1 granules (Figs. S2 F and S3 B). These experiments demonstrate that Syt isoforms do have graded responses to KCl. In biochemical assays, the Syt cytoplasmic domains are predicted to vary by greater than 10-fold in their $Ca^{2+}$ affinities (Hui et al., 2005; Wang et al., 2005), but it is not clear that the observed KCl responses are due to differential $Ca^{2+}$ sensitivity in Syt-1 and Syt-7.

We sought to confirm the $Ca^{2+}$ dependence of graded, Syt-mediated fusion by adjusting, incrementally, the level of $Ca^{2+}$ in the cytosol. To precisely control cytosolic $Ca^{2+}$, the cells were permeabilized by a brief incubation with digitonin and perfused with bath solutions containing 1–100 µM $Ca^{2+}$. We first calculated the fusion probabilities of Syt granule populations as a function of [$Ca^{2+}$] (Fig. 8 A). At concentrations of 1 µM $Ca^{2+}$ or less, fusion of Syt-1 granules is almost completely absent, while fusion of Syt-7 granules is reliably detected. $Ca^{2+}$ must be elevated to 5 µM and higher to observe any Syt-1 granule fusion events. At much higher $Ca^{2+}$ levels (30 and 100 µM), docked granules fuse with roughly equivalent probability. We next plotted individual fusion times of granules bearing Syt-1 or Syt-7 GFP. Histograms for Syt-1 and Syt-7 granule fusion kinetics are significantly shifted to the left as $Ca^{2+}$ is increased (Fig. 8, B and C). Rate constants from single-exponential curves fit to the histograms are shown in Fig. 8 D. The data indicate that Syt-1 activation kinetics are more sensitive to increases in $Ca^{2+}$ than are activation kinetics for Syt-7. As $Ca^{2+}$ increases from 10 to 100 µM, first-order rate constants increase fourfold for Syt-1 and only twofold for Syt-7. At the higher $Ca^{2+}$ concentrations, Syt-1 granules fused more rapidly than Syt-7 granules (Fig. 8 D).

## DISCUSSION

The idea that the dynamics of the chromaffin cell secretory response may be determined by the properties of individual granules was previously posited by Chow and colleagues (Duncan et al., 2003). Using time-resolved

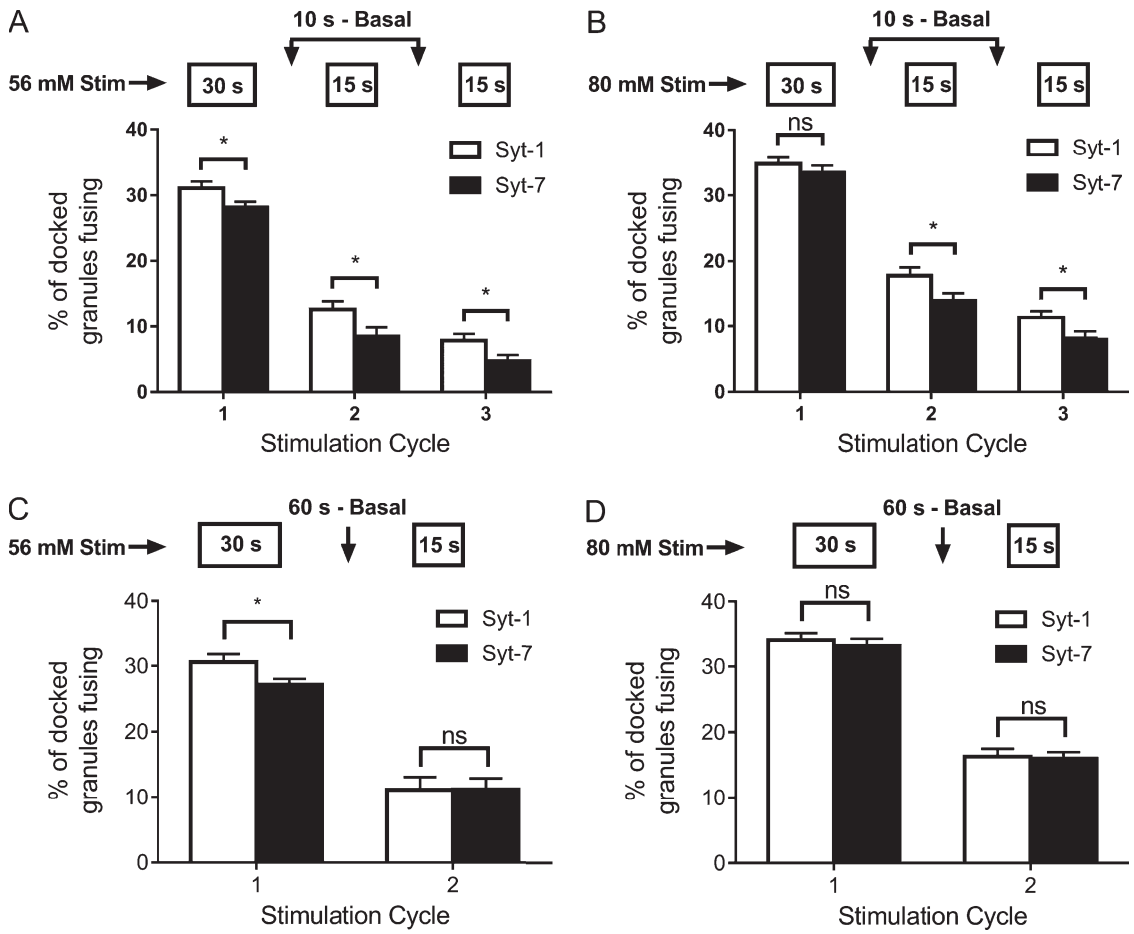


Figure 7. **The effect of repeated stimulation on Syt granule fusion.** Chromaffin cells transfected with Syt-1 or Syt-7 GFP were depolarized with 56 or 80 mM KCl during multiple rounds of stimulation (depicted at the top of each graph). (A and B) Bar graphs represent the percentage of fusing Syt-1 and Syt-7 GFP granules after stimulation with 56 or 80 mM KCl with a shorter intermittent recovery period (10-s interval). The percentage of fusing Syt-1 or Syt-7 GFP granules is based on the total number of docked granules present in the evanescent field before the start of stimulation. Differences between groups were assessed using Student's *t* test ($n$ = 17 cells [56 mM KCl] and $n$ = 12 cells [80 mM KCl]; *, $P < 0.05$). A higher percentage of Syt-1 granules fuse during subsequent stimulations in comparison to Syt-7 granules. Error bars represent SEM. (C and D) Bar graph represents the percentage of fusing Syt-1 or Syt-7 GFP granules during application of 56 or 80 mM KCl with a longer recovery period (60 s). Differences between the groups were assessed using Student's *t* test ($n$ = 17 cells [56 mM KCl] and $n$ = 12 cells [80 mM KCl]; *, $P < 0.05$). Fusion occurred with identical probabilities for both Syt-1 and Syt-7 granules when the recovery period was longer. Error bars represent SEM.

optical imaging, their work suggested that chromaffin granules are segregated spatially and functionally in ways that may reflect sorting to slowly releasable and readily releasable pools. Before this work, the notion of functionally segregated granule pools had largely been inferred from the kinetics of membrane capacitance increases in response to flash uncaging of $Ca^{2+}$ or strong electrophysiological stimulation (Heinemann et al., 1993, 1994).

In this study, we identified several differences in the functional properties of chromaffin granules that could be attributed specifically to the selective sorting of Syt. Among these is the finding that Syt-1 and Syt-7 differ significantly in their activation kinetics in response to membrane depolarization. With a strong stimulus (56 or 80 mM KCl), Syt-7 granules fused with faster kinetics than Syt-1 granules in the same cell (Fig. 1). This observation was made in cells coexpressing isoforms fused to pH-sensitive fluorescent tags (pHuji and pHluorin). The kinetics of activation and fusion were highly sensitive to $Ca^{2+}$. We showed this in two ways: (1) by selective inhibition of voltage-gated channels and (2) by application of $Ca^{2+}$ after membrane permeabilization. The channel blockade experiments demonstrated that the Syts were not equally dependent on $Ca^{2+}$ channel subtypes for fusion. Given the highly localized nature of ion channel–mediated [$Ca^{2+}$] changes, this result suggested that Syt-1 and Syt-7 do not share the same distribution with respect to channels. This is indicated by the fact that channel inhibition did not have identical effects on the fusion probability of Syt-1 and Syt-7 granules. It should be noted that the degree to which

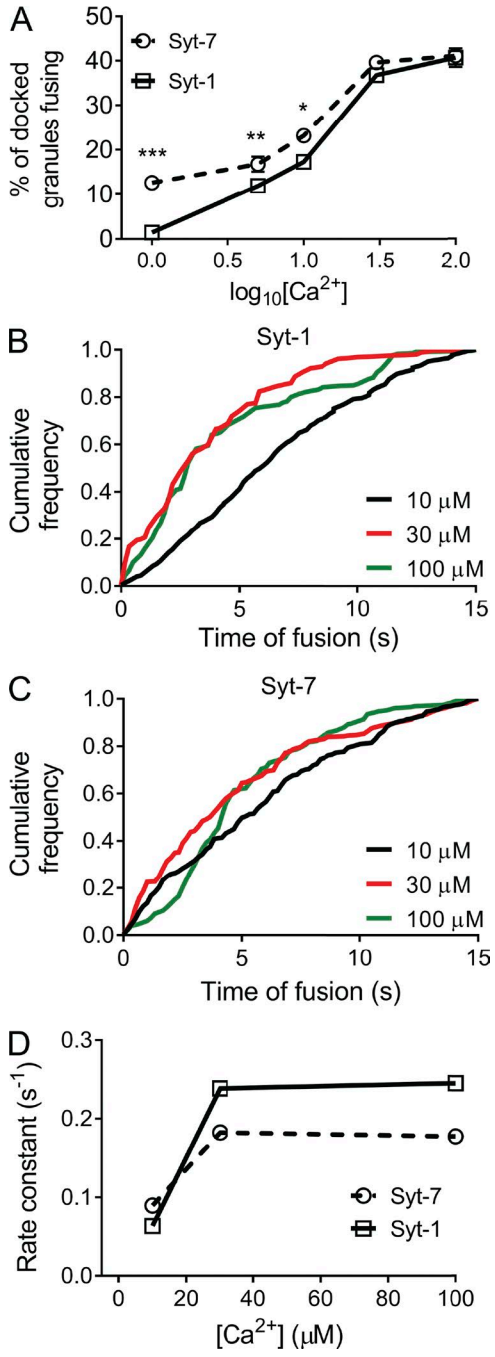


Figure 8. **$Ca^{2+}$-dependence of fusion in permeabilized cells.** Syt-1 or Syt-7 was expressed either as a GFP or pHluorin fusion proteins, separately, in chromaffin cells. Cells were stimulated for 30 s. (A) Fusion efficiency of Syt-1 and Syt-7 granules for each [$Ca^{2+}$]. Raw counts of number of fusion events/number of docked granules are as follows: for Syt-1, 27/1,993 from $n$ = 15 cells (1 µM), 241/1,996 from $n$ = 15 cells (5 µM), 346/2,037 from $n$ = 15 cells (10 µM), 823/2,187 from $n$ = 15 cells (30 µM), and 352/856 $n$ = 10 cells (100 µM); for Syt-7, 318/2,393 from $n$ = 15 cells (1 µM), 368/2,227 from $n$ = 15 cells (5 µM), 491/2,091 from $n$ = 15 cells (10 µM), 811/2,110 from $n$ = 15 cells (30 µM), and 366/894 from $n$ = 10 cells (100 µM). Statistical differences for the percentage fusion of Syt-1 and Syt-7 granules were assessed using Student's $t$ test and were significantly different at [$Ca^{2+}$] of 1 µM (***, $P < 0.001$), 5 µM (**, $P < 0.01$), 10 µM (*, $P < 0.05$), and 30 and 100 µM (ns, $P > 0.05$). (B and C) Cumulative frequency histograms showing the times of fusion of individual Syt-1 and Syt-7 granules (within 15 s of stimulation). (D) Comparison of the rate constants for Syt-1 and Syt-7 granule fusion. Rate constants were determined by fitting single-phase exponential curves to the data in A at 10, 30, and 100 µM $Ca^{2+}$. Syt-1 rate constants at 10, 30, and 100 µM are 0.063, 0.24, and 0.25 $s^{-1}$, respectively. For Syt-1, the 5-µM data could not be fit by a curve. Syt-7 rate constants at 5, 10, 30, and 100 µM are 0.029, 0.090, 0.18, and 0.18 $s^{-1}$.

exocytosis is inhibited (Fig. 2 B) is not well correlated with the degree to which $Ca^{2+}$ fluorescence is reduced by the channel blockers (Fig. 2 A). Although each of the blockers reduced $Ca^{2+}$ fluorescence by roughly threefold, the percentage reduction in fusion was more variable. This may have been because of differences in the overexpression of GCaMP in cells, differences in the channels' relative contribution to exocytosis, or differences in the localization of isoforms with respect to channels. These possibilities are also not mutually exclusive. Interestingly, although nifedipine and GVIA both inhibit exocytosis, the fusion kinetics of Syt-1 and Syt-7 were essentially unaffected. The most dramatic effects on exocytosis were observed with MVIIC, in terms of both fusion inhibition and slowing of fusion kinetics. For Syt-1, the rate constant in the presence of MVIIC was slowed to 39.2 $s^{-1}$ from 20.1 $s^{-1}$; for Syt-7, the rate constant with MVIIC was slowed to 8.6 $s^{-1}$ from 6.1 $s^{-1}$. It is not obvious why the N/P/Q-type blocker MVIIC had such dramatic effects on fusion kinetics but not the N-type blocker GVIA. One explanation may be tighter coupling of P/Q channels with granules (Lara et al., 1998). As a consequence of blocking these channels, exocytosis must be triggered by $Ca^{2+}$ sources farther away, thereby slowing fusion kinetics. In bovine chromaffin cells, P/Q-type channels carry the largest proportion of total $Ca^{2+}$ current (50%), while N- and L-type carry 30% and 20% current, respectively (García et al., 2006). Numerous in vitro studies have also shown that Syt-1 can directly bind to P/Q-, N-, and L-type $Ca^{2+}$ channels (Charvin et al., 1997; Sheng et al., 1997; Wiser et al., 1999; Rosa et al., 2011; Mahapatra et al., 2012). One can speculate that Syt-1 granules are localized closer to $Ca^{2+}$ channels to compensate for their relatively low $Ca^{2+}$-binding affinity (Hui et al., 2005; Bhalla et al., 2008). In contrast, multiple in vitro studies demonstrate that Syt-7's $Ca^{2+}$ sensitivity for binding membranes exceeds that of Syt-1 by more than an order of magnitude (Hui et al., 2005; Wang et al., 2005; Bhalla et al., 2008). Syt-7 granules may thus not be as dependent on close coupling to $Ca^{2+}$ channels because of Syt-7's higher $Ca^{2+}$ sensitivity versus that of Syt-1.

Interestingly, we do find evidence for geographic differences in preferred fusion locations of Syt-1 and Syt-7 granules. Syt-7 granules tend to fuse in locations

that deviate significantly from random, consistent with clustering. On the other hand, Syt-1 granules tend to show no such fusion location bias (Fig. 3). What this means from a molecular perspective is not yet clear. It may well reflect a level of organization that places particular granule populations close to specific channels or components of the fusion machinery. The analysis approach developed in this study will be useful to interrogating this issue in subsequent studies. Indeed, this analysis approach may be broadly useful to study the clustering (or anticlustering) of proteins or protein complexes important for dynamic cellular processes of the kind described here.

Syt-7 granules are less mobile than Syt-1 granules and fuse with faster kinetics when depolarized with KCl (Fig. 1). One might assume that this satisfies the conditions of Syt-7 granules' belonging to a "docked" and "primed" population. However, even with a strongly depolarizing KCl stimulus (100 mM KCl), we estimate that the $[Ca^{2+}]_i$ saturates at only ∼5 µM in the subplasmalemma (Fig. S1). This does not approach the typically much higher concentrations of $Ca^{2+}$ used in flash uncaging experiments (Schonn et al., 2008). In permeabilized cells, when cytosolic $Ca^{2+}$ was elevated to concentrations that exceeded 30 µM, Syt-1 granule fusion kinetics were faster than those for Syt-7 (Fig. 8). As such, the faster kinetics observed for Syt-7 granules under KCl stimulation may directly result from Syt-7's higher calcium affinity rather than a tendency toward "docked" or "primed" states. It should be noted that the proportion of docked granules that fuse with high KCl depolarization (Fig. S3 B) and with "matched" concentrations of $Ca^{2+}$ in permeabilized cells (Fig. 8 A) are not identical. However, regardless of the method used to elicit exocytosis, there is a clear distinction in the secretory responses of Syt-1 and Syt-7 granules. Small elevations from baseline in cytosolic $Ca^{2+}$ are generally ineffective at driving fusion of granules bearing Syt-1 and much more effective at driving fusion of granules bearing Syt-7. This is again consistent with prior in vitro studies, which demonstrate that Syt-7 binds membranes and triggers fusion at far lower $Ca^{2+}$ concentrations as compared Syt-1(Hui et al., 2005; Wang et al., 2005; Bhalla et al., 2008). As $Ca^{2+}$ rises (in cells, ostensibly as a result of membrane depolarization), both populations of granules fuse with higher efficacy (Fig. 8 A). These results strongly suggest that the differences in Syt-1 and Syt-7 granule fusion are mediated by differential $Ca^{2+}$-phospholipid affinities between the two isoforms.

Our data also show that not all granules that undergo fusion are present in the evanescent field before stimulation. Moreover, these newly arriving vesicles or "newcomers" have distinct properties depending on their corresponding Syt isoform. Our study indicated that a larger proportion of fusing Syt-1 granules are newcomers in comparison to Syt-7 (Fig. 5). In order for a newcomer granule to undergo fusion, it must first undergo interactions with proteins at the plasma membrane, including t-SNAREs. These interactions are well characterized in chromaffin cells and are believed to be mediated in part by the activity of Munc18-1. For example, using Munc18-1 knockout mice, Neher and colleagues showed that lack of Munc18-1 dramatically reduced the proportion of granules docked at the plasma membrane (Voets et al., 2001b). A more recent study found that overexpression of syntaxin-3 (Syn-3) in INS-1 cells resulted in increased recruitment of newcomer granules during stimulation (Zhu et al., 2013). A possible explanation for our findings is thus that Syt-1 granules have a higher affinity for proteins such as Munc18-1 and/or Syn-3 that mediate rapid recruitment of granules from within the cell. However, not much is known regarding isoform-specific interactions of Syts and SNAREs/SMs that impinge on the late steps of exocytosis.

Two points with regard to spatial and temporal resolution of these studies should be noted. First, although we do find that Syt granules are located at different distances from the membrane, our ability to reliably resolve those distances may be limited by the thickness of the confocal sections. Alternative imaging approaches, such as electron microscopy or stochastic optical reconstruction microscopy, may allow higher resolution measurements of distance from the membrane. Second, there appears to be no upper limit (at least within our imaging time resolution) to how quickly a granule can fuse after initially entering the evanescent field. This raises questions about what constitutes docking from a molecular and even morphological perspective. In this study we apply a phenomenological definition of docking that only requires a granule to be present in the evanescent field at the start of stimulation.

The distinct, $Ca^{2+}$-dependent properties of chromaffin granules shown here indicate that Syt mediates differences in the behavior of individual secretory granules in an isoform-specific manner. These differences provide a molecular framework for the mechanisms that underlie stimulus specificity of secretion. In particular, the ubiquity of $Ca^{2+}$ as a secretory switch demands a highly tuned set of $Ca^{2+}$ sensors for exocytosis. Our work suggests that Syt-1 and Syt-7, via distinct trafficking pathways and graded $Ca^{2+}$ affinities, allow tunable responses to a wide range of stimuli that differentially elevate intracellular $Ca^{2+}$.

## ACKNOWLEDGMENTS

We would like to thank Mary Bittner for assistance on the digitonin permeabilization experiments and Ronald Holz for helpful suggestions on many of the experiments that were conducted. We also thank Dr. Lawrence G. Palmer for providing helpful feedback on the manuscript.

This research was supported by the National Institutes of Health (grant GM111997 to A. Anantharam, grant GM110289 to

D. Axelrod, and grant MH061876 to E.R. Chapman), the American Heart Association (grant SDG14420049 to A. Anantharam), and the Richard Barber Summer Research Program (to A. Anantharam, T.C. Rao, and P.J. Dahl). E.R. Chapman is an investigator of the Howard Hughes Medical Institute.

The authors declare no competing financial interests.

Angus C. Nairn served as editor.

Submitted: 16 January 2017
Revised: 15 May 2017
Accepted: 12 June 2017

## REFERENCES

Akerboom, J., T.W. Chen, T.J. Wardill, L. Tian, J.S. Marvin, S. Mutlu, N.C. Calderón, F. Esposti, B.G. Borghuis, X.R. Sun, et al. 2012. Optimization of a GCaMP calcium indicator for neural activity imaging. *J. Neurosci.* 32:13819–13840. http://dx.doi.org/10.1523/JNEUROSCI.2601-12.2012

Allersma, M.W., L. Wang, D. Axelrod, and R.W. Holz. 2004. Visualization of regulated exocytosis with a granule-membrane probe using total internal reflection microscopy. *Mol. Biol. Cell.* 15:4658–4668. http://dx.doi.org/10.1091/mbc.E04-02-0149

Augustine, G.J., and E. Neher. 1992. Calcium requirements for secretion in bovine chromaffin cells. *J. Physiol.* 450:247–271. http://dx.doi.org/10.1113/jphysiol.1992.sp019126

Bacaj, T., D. Wu, X. Yang, W. Morishita, P. Zhou, W. Xu, R.C. Malenka, and T.C. Südhof. 2013. Synaptotagmin-1 and synaptotagmin-7 trigger synchronous and asynchronous phases of neurotransmitter release. *Neuron.* 80:947–959. http://dx.doi.org/10.1016/j.neuron.2013.10.026

Bal, M., J. Leitz, A.L. Reese, D.M. Ramirez, M. Durakoglugil, J. Herz, L.M. Monteggia, and E.T. Kavalali. 2013. Reelin mobilizes a VAMP7-dependent synaptic vesicle pool and selectively augments spontaneous neurotransmission. *Neuron.* 80:934–946. http://dx.doi.org/10.1016/j.neuron.2013.08.024

Bhalla, A., W.C. Tucker, and E.R. Chapman. 2005. Synaptotagmin isoforms couple distinct ranges of Ca2+, Ba2+, and Sr2+ concentration to SNARE-mediated membrane fusion. *Mol. Biol. Cell.* 16:4755–4764. http://dx.doi.org/10.1091/mbc.E05-04-0277

Bhalla, A., M.C. Chicka, and E.R. Chapman. 2008. Analysis of the synaptotagmin family during reconstituted membrane fusion. Uncovering a class of inhibitory isoforms. *J. Biol. Chem.* 283:21799–21807. http://dx.doi.org/10.1074/jbc.M709628200

Bittner, M.A., and R.W. Holz. 1992. Kinetic analysis of secretion from permeabilized adrenal chromaffin cells reveals distinct components. *J. Biol. Chem.* 267:16219–16225.

Brose, N., A.G. Petrenko, T.C. Südhof, and R. Jahn. 1992. Synaptotagmin: a calcium sensor on the synaptic vesicle surface. *Science.* 256:1021–1025. http://dx.doi.org/10.1126/science.1589771

Campbell, T.N., and F.Y. Choy. 2001. The effect of pH on green fluorescent protein: a brief review. *Mol. Biol. Today.* 2:1–4.

Chapman, E.R. 2002. Synaptotagmin: a Ca(2+) sensor that triggers exocytosis? *Nat. Rev. Mol. Cell Biol.* 3:498–508. http://dx.doi.org/10.1038/nrm855

Charvin, N., C. L'evêque, D. Walker, F. Berton, C. Raymond, M. Kataoka, Y. Shoji-Kasai, M. Takahashi, M. De Waard, and M.J. Seagar. 1997. Direct interaction of the calcium sensor protein synaptotagmin I with a cytoplasmic domain of the alpha1A subunit of the P/Q-type calcium channel. *EMBO J.* 16:4591–4596. http://dx.doi.org/10.1093/emboj/16.15.4591

Chen, T.-W., T.J. Wardill, Y. Sun, S.R. Pulver, S.L. Renninger, A. Baohan, E.R. Schreiter, R.A. Kerr, M.B. Orger, V. Jayaraman, et al. 2013. Ultrasensitive fluorescent proteins for imaging neuronal activity. *Nature.* 499:295–300. http://dx.doi.org/10.1038/nature12354

Crawford, D.C., and E.T. Kavalali. 2015. Molecular underpinnings of synaptic vesicle pool heterogeneity. *Traffic.* 16:338–364. http://dx.doi.org/10.1111/tra.12262

de Diego, A.M., L. Gandía, and A.G. García. 2008. A physiological view of the central and peripheral mechanisms that regulate the release of catecholamines at the adrenal medulla. *Acta Physiol. (Oxf.).* 192:287–301. http://dx.doi.org/10.1111/j.1748-1716.2007.01807.x

Degtyar, V.E., M.W. Allersma, D. Axelrod, and R.W. Holz. 2007. Increased motion and travel, rather than stable docking, characterize the last moments before secretory granule fusion. *Proc. Natl. Acad. Sci. USA.* 104:15929–15934. http://dx.doi.org/10.1073/pnas.0705406104

Douglas, W.W., and R.P. Rubin. 1961. The role of calcium in the secretory response of the adrenal medulla to acetylcholine. *J. Physiol.* 159:40–57. http://dx.doi.org/10.1113/jphysiol.1961.sp006791

Duncan, R.R., J. Greaves, U.K. Wiegand, I. Matskevich, G. Bodammer, D.K. Apps, M.J. Shipston, and R.H. Chow. 2003. Functional and spatial segregation of secretory vesicle pools according to vesicle age. *Nature.* 422:176–180. http://dx.doi.org/10.1038/nature01389

Fernandez, I., D. Araç, J. Ubach, S.H. Gerber, O. Shin, Y. Gao, R.G. Anderson, T.C. Südhof, and J. Rizo. 2001. Three-dimensional structure of the synaptotagmin 1 C2B-domain: synaptotagmin 1 as a phospholipid binding machine. *Neuron.* 32:1057–1069. http://dx.doi.org/10.1016/S0896-6273(01)00548-7

Fernández-Alfonso, T., R. Kwan, and T.A. Ryan. 2006. Synaptic vesicles interchange their membrane proteins with a large surface reservoir during recycling. *Neuron.* 51:179–186. http://dx.doi.org/10.1016/j.neuron.2006.06.008

Fulop, T., and C. Smith. 2007. Matching native electrical stimulation by graded chemical stimulation in isolated mouse adrenal chromaffin cells. *J. Neurosci. Methods.* 166:195–202. http://dx.doi.org/10.1016/j.jneumeth.2007.07.004

García, A.G., A.M. García-De-Diego, L. Gandía, R. Borges, and J. García-Sancho. 2006. Calcium signaling and exocytosis in adrenal chromaffin cells. *Physiol. Rev.* 86:1093–1131. http://dx.doi.org/10.1152/physrev.00039.2005

Giovannucci, D.R., and E.L. Stuenkel. 1997. Regulation of secretory granule recruitment and exocytosis at rat neurohypophysial nerve endings. *J. Physiol.* 498:735–751. http://dx.doi.org/10.1113/jphysiol.1997.sp021898

Heinemann, C., L. von Rüden, R.H. Chow, and E. Neher. 1993. A two-step model of secretion control in neuroendocrine cells. *Pflugers Arch.* 424:105–112. http://dx.doi.org/10.1007/BF00374600

Heinemann, C., R.H. Chow, E. Neher, and R.S. Zucker. 1994. Kinetics of the secretory response in bovine chromaffin cells following flash photolysis of caged Ca2+. *Biophys. J.* 67:2546–2557. http://dx.doi.org/10.1016/S0006-3495(94)80744-1

Hernández-Guijo, J.M., R. de Pascual, A.G. García, and L. Gandía. 1998. Separation of calcium channel current components in mouse chromaffin cells superfused with low- and high-barium solutions. *Pflugers Arch.* 436:75–82. http://dx.doi.org/10.1007/s004240050606

Hui, E., J. Bai, P. Wang, M. Sugimori, R.R. Llinas, and E.R. Chapman. 2005. Three distinct kinetic groupings of the synaptotagmin family: candidate sensors for rapid and delayed exocytosis. *Proc. Natl. Acad. Sci. USA.* 102:5210–5214. http://dx.doi.org/10.1073/pnas.0500941102

Kneen, M., J. Farinas, Y. Li, and A.S. Verkman. 1998. Green fluorescent protein as a noninvasive intracellular pH indicator.

*Biophys. J.* 74:1591–1599. http://dx.doi.org/10.1016/S0006-3495(98)77870-1

Lara, B., L. Gandía, R. Martínez-Sierra, A. Torres, and A.G. García. 1998. Q-type Ca2+ channels are located closer to secretory sites than L-type channels: functional evidence in chromaffin cells. *Pflugers Arch.* 435:472–478. http://dx.doi.org/10.1007/s004240050541

Lee, J., and J.T. Littleton. 2015. Transmembrane tethering of synaptotagmin to synaptic vesicles controls multiple modes of neurotransmitter release. *Proc. Natl. Acad. Sci. USA.* 112:3793–3798.

Luo, F., T. Bacaj, and T.C. Südhof. 2015. Synaptotagmin-7 is essential for Ca2+-triggered delayed asynchronous release but not for Ca2+-dependent vesicle priming in retinal ribbon synapses. *J. Neurosci.* 35:11024–11033. http://dx.doi.org/10.1523/JNEUROSCI.0759-15.2015

Mahapatra, S., C. Calorio, D.H.F. Vandael, A. Marcantoni, V. Carabelli, and E. Carbone. 2012. Calcium channel types contributing to chromaffin cell excitability, exocytosis and endocytosis. *Cell Calcium.* 51:321–330. http://dx.doi.org/10.1016/j.ceca.2012.01.005

Maravall, M., Z.F. Mainen, B.L. Sabatini, and K. Svoboda. 2000. Estimating intracellular calcium concentrations and buffering without wavelength ratioing. *Biophys. J.* 78:2655–2667. http://dx.doi.org/10.1016/S0006-3495(00)76809-3

Neher, E. 1995. The use of fura-2 for estimating Ca buffers and Ca fluxes. *Neuropharmacology.* 34:1423–1442. http://dx.doi.org/10.1016/0028-3908(95)00144-U

Neher, E., and G.J. Augustine. 1992. Calcium gradients and buffers in bovine chromaffin cells. *J. Physiol.* 450:273–301. http://dx.doi.org/10.1113/jphysiol.1992.sp019127

Passmore, D.R., T.C. Rao, A.R. Peleman, and A. Anantharam. 2014. Imaging plasma membrane deformations with pTIRFM. *J. Vis. Exp.* (86):51334. http://dx.doi.org/10.3791/51334

Perin, M.S., V.A. Fried, G.A. Mignery, R. Jahn, and T.C. Südhof. 1990. Phospholipid binding by a synaptic vesicle protein homologous to the regulatory region of protein kinase C. *Nature.* 345:260–263. http://dx.doi.org/10.1038/345260a0

Perin, M.S., P.A. Johnston, T. Ozcelik, R. Jahn, U. Francke, and T.C. Südhof. 1991. Structural and functional conservation of synaptotagmin (p65) in Drosophila and humans. *J. Biol. Chem.* 266:615–622.

Raingo, J., M. Khvotchev, P. Liu, F. Darios, Y.C. Li, D.M. Ramirez, M. Adachi, P. Lemieux, K. Toth, B. Davletov, and E.T. Kavalali. 2012. VAMP4 directs synaptic vesicles to a pool that selectively maintains asynchronous neurotransmission. *Nat. Neurosci.* 15:738–745. http://dx.doi.org/10.1038/nn.3067

Rao, T.C., D.R. Passmore, A.R. Peleman, M. Das, E.R. Chapman, and A. Anantharam. 2014. Distinct fusion properties of synaptotagmin-1 and synaptotagmin-7 bearing dense core granules. *Mol. Biol. Cell.* 25:2416–2427. http://dx.doi.org/10.1091/mbc.E14-02-0702

Rosa, J.M., C.J. Torregrosa-Hetland, I. Colmena, L.M. Gutiérrez, A.G. García, and L. Gandía. 2011. Calcium entry through slow-inactivating L-type calcium channels preferentially triggers endocytosis rather than exocytosis in bovine chromaffin cells. *Am. J. Physiol. Cell Physiol.* 301:C86–C98. http://dx.doi.org/10.1152/ajpcell.00440.2010

Schonn, J.S., A. Maximov, Y. Lao, T.C. Südhof, and J.B. Sørensen. 2008. Synaptotagmin-1 and -7 are functionally overlapping Ca2+ sensors for exocytosis in adrenal chromaffin cells. *Proc. Natl. Acad. Sci. USA.* 105:3998–4003. http://dx.doi.org/10.1073/pnas.0712373105

Shen, Y., M. Rosendale, R.E. Campbell, and D. Perrais. 2014. pHuji, a pH-sensitive red fluorescent protein for imaging of exo- and endocytosis. *J. Cell Biol.* 207:419–432. http://dx.doi.org/10.1083/jcb.201404107

Sheng, Z.-H., C.T. Yokoyama, and W.A. Catterall. 1997. Interaction of the synprint site of N-type Ca2+ channels with the C2B domain of synaptotagmin I. *Proc. Natl. Acad. Sci. USA.* 94:5405–5410. http://dx.doi.org/10.1073/pnas.94.10.5405

Sørensen, J.B. 2004. Formation, stabilisation and fusion of the readily releasable pool of secretory vesicles. *Pflugers Arch.* 448:347–362. http://dx.doi.org/10.1007/s00424-004-1247-8

Südhof, T.C., and J. Rizo. 1996. Synaptotagmins: C2-domain proteins that regulate membrane traffic. *Neuron.* 17:379–388. http://dx.doi.org/10.1016/S0896-6273(00)80171-3

Sugita, S., O.H. Shin, W. Han, Y. Lao, and T.C. Südhof. 2002. Synaptotagmins form a hierarchy of exocytotic Ca(2+) sensors with distinct Ca(2+) affinities. *EMBO J.* 21:270–280. http://dx.doi.org/10.1093/emboj/21.3.270

Sutton, R.B., B.A. Davletov, A.M. Berghuis, T.C. Südhof, and S.R. Sprang. 1995. Structure of the first C2 domain of synaptotagmin I: a novel Ca2+/phospholipid-binding fold. *Cell.* 80:929–938. http://dx.doi.org/10.1016/0092-8674(95)90296-1

Tsien, R.Y. 1998. The green fluorescent protein. *Annu. Rev. Biochem.* 67:509–544. http://dx.doi.org/10.1146/annurev.biochem.67.1.509

Ubach, J., X. Zhang, X. Shao, T.C. Südhof, and J. Rizo. 1998. Ca2+ binding to synaptotagmin: how many Ca2+ ions bind to the tip of a C2-domain? *EMBO J.* 17:3921–3930. http://dx.doi.org/10.1093/emboj/17.14.3921

Voets, T. 2000. Dissection of three Ca2+-dependent steps leading to secretion in chromaffin cells from mouse adrenal slices. *Neuron.* 28:537–545. http://dx.doi.org/10.1016/S0896-6273(00)00131-8

Voets, T., E. Neher, and T. Moser. 1999. Mechanisms underlying phasic and sustained secretion in chromaffin cells from mouse adrenal slices. *Neuron.* 23:607–615. http://dx.doi.org/10.1016/S0896-6273(00)80812-0

Voets, T., T. Moser, P.E. Lund, R.H. Chow, M. Geppert, T.C. Südhof, and E. Neher. 2001a. Intracellular calcium dependence of large dense-core vesicle exocytosis in the absence of synaptotagmin I. *Proc. Natl. Acad. Sci. USA.* 98:11680–11685. http://dx.doi.org/10.1073/pnas.201398798

Voets, T., R.F. Toonen, E.C. Brian, H. de Wit, T. Moser, J. Rettig, T.C. Südhof, E. Neher, and M. Verhage. 2001b. Munc18-1 promotes large dense-core vesicle docking. *Neuron.* 31:581–591. http://dx.doi.org/10.1016/S0896-6273(01)00391-9

Walter, A.M., A.J. Groffen, J.B. Sørensen, and M. Verhage. 2011. Multiple Ca2+ sensors in secretion: teammates, competitors or autocrats? *Trends Neurosci.* 34:487–497. http://dx.doi.org/10.1016/j.tins.2011.07.003

Wang, P., M.C. Chicka, A. Bhalla, D.A. Richards, and E.R. Chapman. 2005. Synaptotagmin VII is targeted to secretory organelles in PC12 cells, where it functions as a high-affinity calcium sensor. *Mol. Cell. Biol.* 25:8693–8702. http://dx.doi.org/10.1128/MCB.25.19.8693-8702.2005

Weber, J.P., T.L. Toft-Bertelsen, R. Mohrmann, I. Delgado-Martinez, and J.B. Sørensen. 2014. Synaptotagmin-7 is an asynchronous calcium sensor for synaptic transmission in neurons expressing SNAP-23. *PLoS One.* 9:e114033. http://dx.doi.org/10.1371/journal.pone.0114033

Wick, P.F., R.A. Senter, L.A. Parsels, M.D. Uhler, and R.W. Holz. 1993. Transient transfection studies of secretion in bovine chromaffin cells and PC12 cells. Generation of kainate-sensitive chromaffin cells. *J. Biol. Chem.* 268:10983–10989.

Wiser, O., M. Trus, A. Hernández, E. Renström, S. Barg, P. Rorsman, and D. Atlas. 1999. The voltage sensitive Lc-type Ca2+ channel is functionally coupled to the exocytotic machinery. *Proc. Natl.*

*Acad. Sci. USA*. 96:248–253. http://dx.doi.org/10.1073/pnas.96.1.248

Zhu, D., E. Koo, E. Kwan, Y. Kang, S. Park, H. Xie, S. Sugita, and H.Y. Gaisano. 2013. Syntaxin-3 regulates newcomer insulin granule exocytosis and compound fusion in pancreatic beta cells. *Diabetologia*. 56:359–369. http://dx.doi.org/10.1007/s00125-012-2757-0

Rao et al., https://doi.org/10.1085/jgp.201711757

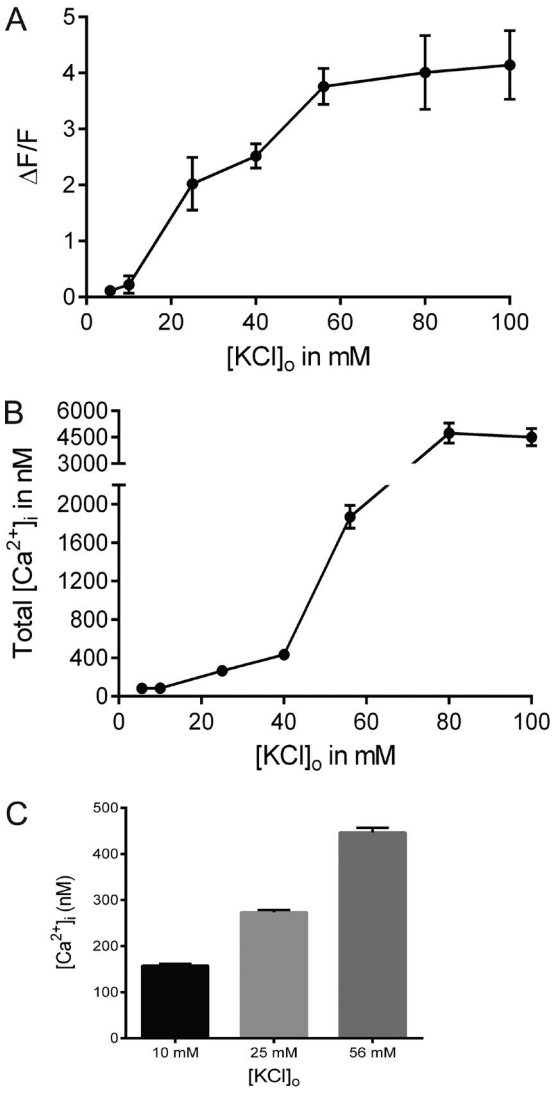


Figure S1. **Determination of $[Ca^{2+}]_i$ in chromaffin cells using TIRF microscopy and patch clamping.** (A) Chromaffin cells transfected with GCaMP5G were stimulated with different levels of extracellular KCl (5.6, 10, 25, 40, 56, 80, and 100 mM) to depolarize the membrane potential. Graph shows the averaged fold changes in GCaMP5G fluorescence (ΔF/F) after KCl depolarization to estimate indicator saturation. Error bars depict SEM ($n$ = 8 cells for each depolarization condition). (B) Graph indicates the total intracellular free $Ca^{2+}$ concentration (nM) after depolarization with KCl. Values were estimated using the equations obtained from Maravall et al. (2000). Error bars depict SEM ($n$ = 8 cells for each condition). (C) Ratiometric $Ca^{2+}$ imaging of chromaffin cells was performed to determine changes in cytosolic free $Ca^{2+}$ evoked by the stimulating solutions (for 10 mM KCl, $n$ = 10 cells; for 25 mM KCl, $n$ = 7 cells; and for 56 mM KCl, $n$ = 5 cells). Patch-clamping was performed at room temperature. Error bars represent SEM.

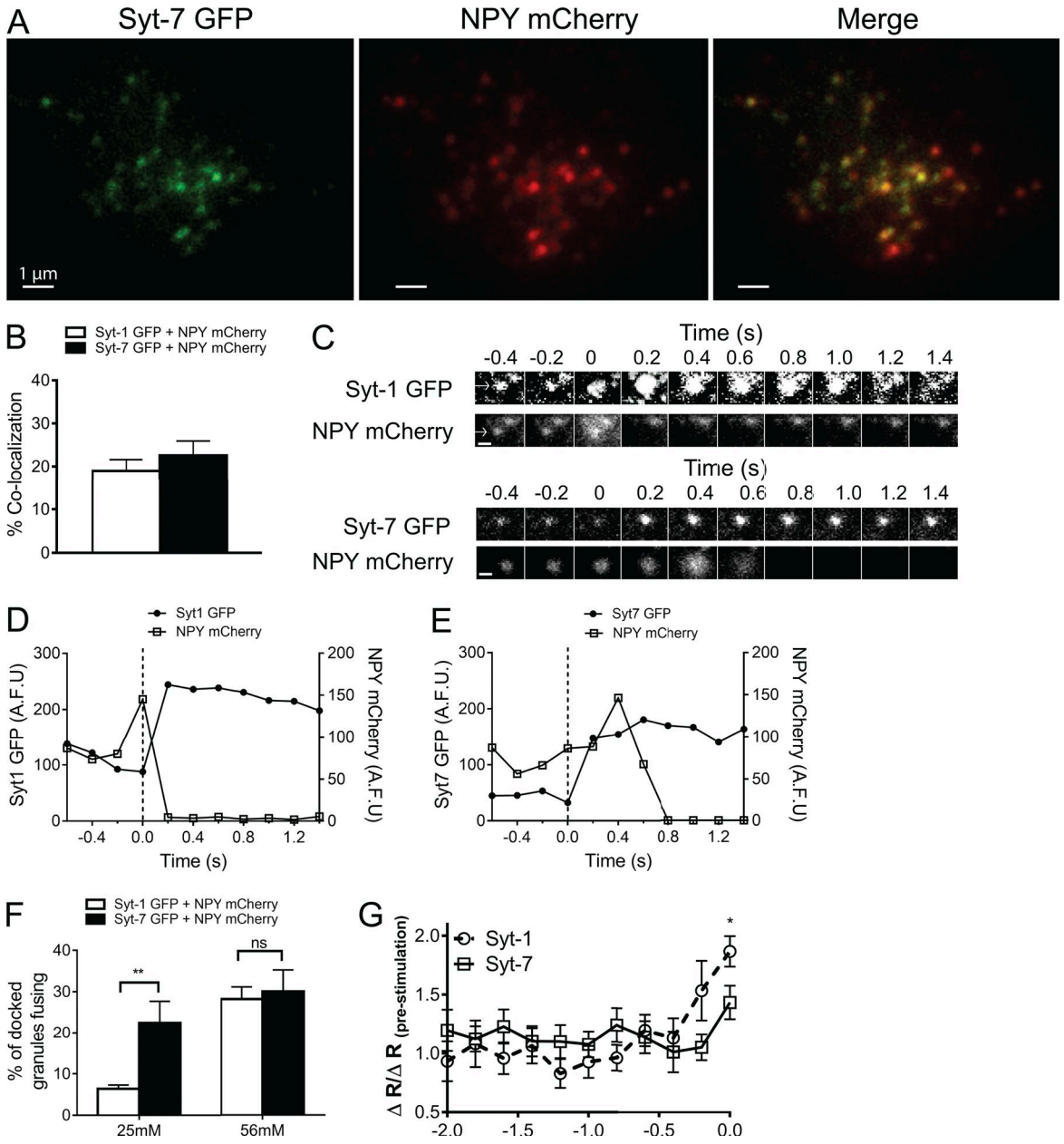


Figure S2. **Dual-color imaging experiments performed to determine mobility and fusion efficacy of granules harboring NPY mCherry and either Syt-1 or Syt-7 GFP.** (A) A chromaffin cell expressing NPY mCherry and Syt-7 GFP. Bars, 1 µm. (B) Percentage colocalization of Syt-1 GFP and NPY Cherry in 14 cells was 19%; for Syt-7 GFP and NPY Cherry, it was 23% (14 cells). Error bars represent SEM. (C) Examples of chromaffin granules bearing both Syt GFP and NPY Cherry undergoing fusion. Arrows indicate the location of the fusing granule. Bars, 300 nm. (D and E) Graphs corresponding the fusion events shown in C. The dotted line at time 0 is the frame before exocytosis. (F) With 25 mM KCl depolarization, 6.4% of docked NPY Cherry granules bearing Syt-1 fused ($n$ = 7), whereas 23% of docked NPY Cherry granules with Syt-7 fused ($n$ = 5). With 56 mM KCl depolarization, 28% of docked NPY Cherry granules with Syt-1 fused ($n$ = 7), whereas 30% of docked NPY Cherry granules with Syt-7 fused ($n$ = 5). **, $P < 0.01$. Error bars represent SEM. (G) Mean frame-to-frame motion of fusing NPY Cherry granules bearing either Syt-1 or Syt-7 in the 2 s before fusion (time 0). Statistical differences were assessed using Student's $t$ test ($n$ = 5 cells, 28 tracks, Syt-7; $n$ = 4 cells, 20 tracks, Syt-1; *, $P < 0.05$). Error bars represent SEM.

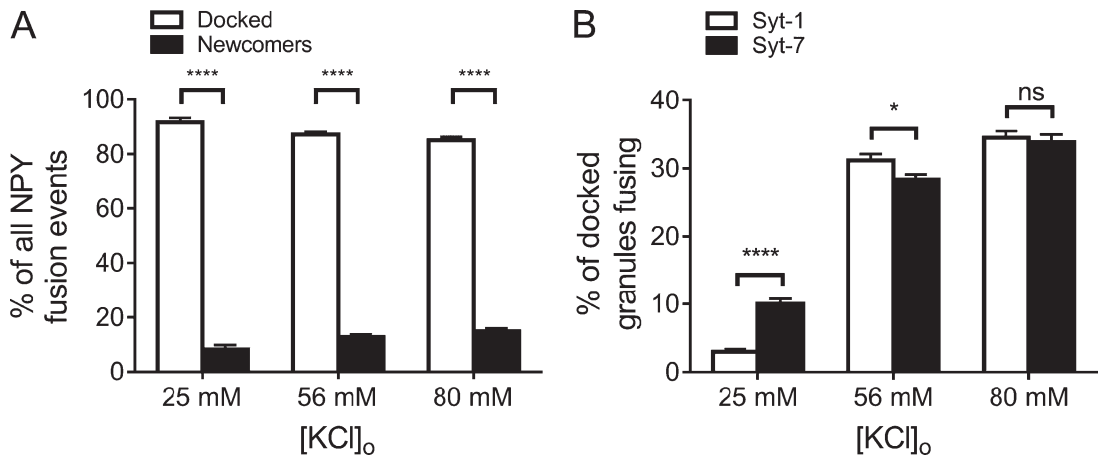


Figure S3. **Stimulation dependence of exocytosis from docked and newcomer Syt-1 or Syt-7 granule populations.** (A) Bar graph depicting the percentage of docked and newcomer NPY-expressing granules that fuse in relation to the total number of fusion events. Statistical differences were assessed using Student's *t* test (****, $P < 0.0001$). Error bars represent SEM. (B) Syt-1 or Syt-7 GFP was expressed separately in chromaffin cells, and exocytosis was triggered by stimulation with KCl of different strengths (25, 56, and 80 mM). Error bars represent SEM. The number of fusing Syt granules for each condition is expressed as a percentage of all granules resident in the evanescent field ("docked") 10 s before the start of the stimulus ($n = 12$ cells [25 and 80 mM KCl]; $n = 18$ [56 mM KCl]). Statistical differences were assessed using Student's *t* test (*, $P < 0.05$; ****, $P < 0.0001$).

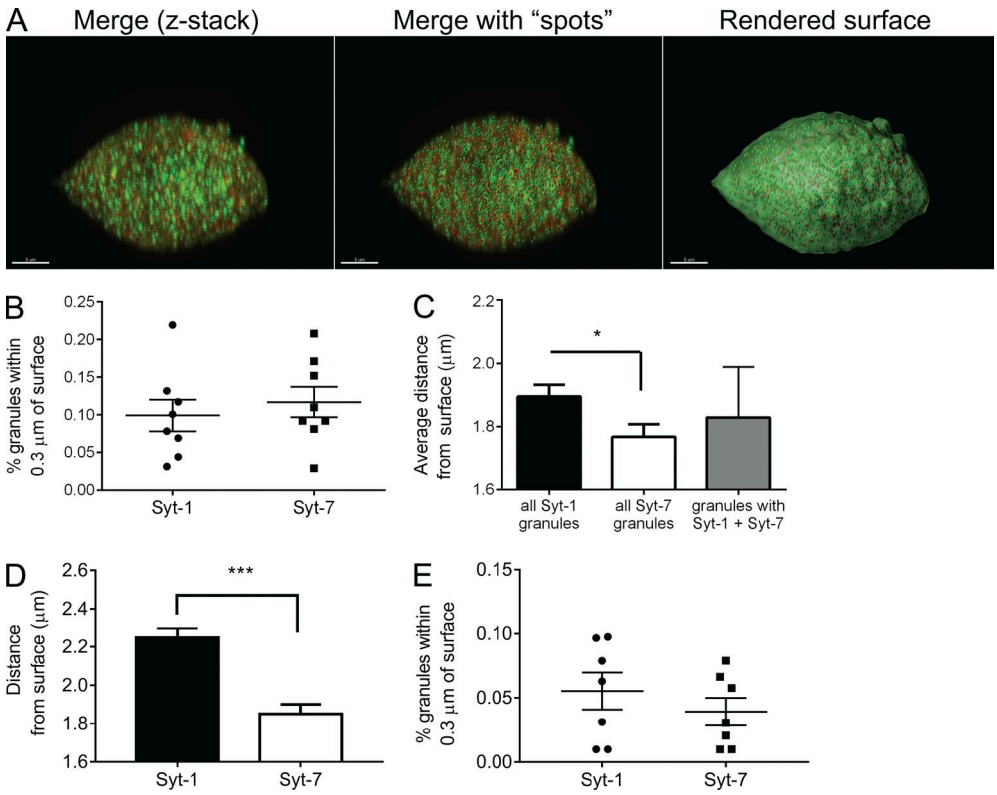


Figure S4. **Distribution of Syt isoforms with respect to a rendered cell surface.** (A) A 3D image of a chromaffin cell reconstructed from individual confocal z-sections (0.71 µm). Antibodies were used to identify endogenous Syt-1 and Syt-7 proteins. The spheres in the middle panel mark stained Syt-1 (red) or Syt-7 (green) puncta (generated using the Spot function in Imaris). Fluorescence emission of the outermost Syt granules was used to roughly demarcate the membrane and render a 3D surface (Imaris). Bars, 5 µm. (B) Graph shows the percentage of Syt-1 or Syt-7 granules located within a distance of one granule diameter (0.3 µm) from the rendered surface ($n$ = 8 cells). (C) The overall mean distances of granules bearing Syt-1, Syt-7, or both isoforms were calculated with reference to the nearest surface. Note that this analysis takes into account all granules, not just those within 0.3 µm of the surface, as in B. Distances of Syt-1 and Syt-7 granules from the membrane are statistically different (Student's $t$ test; *, $P < 0.05$). Error bars represent SEM. (D and E) Graphs based on the analysis of chromaffin cells expressing Syt-1 or Syt-7 GFP and stained with Vybrant DiD. In D, the mean distances of fluorescent puncta from the plasma membrane for six cells are plotted. Distances of Syt-1 and Syt-7 granules from the membrane are statistically different (Student's $t$ test; ***, $P < 0.001$). In E, the graph shows the percentage of Syt-1 or Syt-7 granules located within a distance of one granule diameter (0.3 µm) from the surface. Error bars represent SEM.

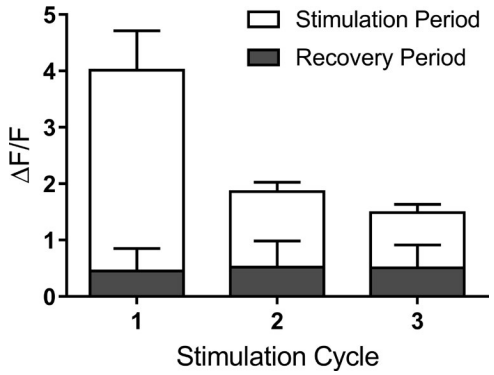


Figure S5. **Effect of repeated stimulation on changes in concentration of near-membrane $Ca^{2+}$ determined using gCaMP5G, a genetically encoded $Ca^{2+}$ indicator, transfected in chromaffin cells and measured using TIRF microscopy.** The bar graph represents the maximum ΔF/F changes during stimulation (56 mM KCl) and the subsequent recovery periods (10 s, $n = 7$ cells). Error bars represent SEM. Changes in GCaMP5G fluorescence were almost 8- to 10-fold higher during the first stimulation period in comparison with the subsequent recovery period. During the second and third periods, there was a three- to fourfold difference in GCaMP5G fluorescence between stimulation and recovery periods. Thus, $Ca^{2+}$ was largely (but not entirely) cleared from the cytosol between stimulation periods.

## REFERENCE

Maravall, M., Z.F. Mainen, B.L. Sabatini, and K. Svoboda. 2000. Estimating intracellular calcium concentrations and buffering without wavelength ratioing. *Biophys. J.* 78:2655–2667. http://dx.doi.org/10.1016/S0006-3495(00)76809-3